Discovery of glycerol phosphate modification on streptococcal rhamnose polysaccharides

Rebecca J. Edgar[1], Vincent P. van Hensbergen[2, #], Alessandro Ruda[3, #], Andrew G. Turner[4], Pan Deng[5], Yoann Le Breton[6], Najib M. El-Sayed[6,7], Ashton T. Belew[6,7], Kevin S. McIver[6], Alastair G. McEwan[4], Andrew J. Morris[5], Gérard Lambeau[8], Mark J. Walker[4], Jeffrey S. Rush[1], Konstantin V. Korotkov[1], Göran Widmalm[3], Nina M. van Sorge[2,§,*], and Natalia Korotkova[1, §,*]

[1]Department of Molecular and Cellular Biochemistry, University of Kentucky, Lexington, Kentucky, USA

[2]Department of Medical Microbiology, University Medical Center Utrecht, Utrecht University, Utrecht, The Netherlands

[3]Department of Organic Chemistry, Arrhenius Laboratory, Stockholm University, Stockholm, Sweden

[4]Australian Infectious Diseases Research Centre and School of Chemistry and Molecular Biosciences, The University of Queensland, Brisbane, Australia

[5]Division of Cardiovascular Medicine and the Gill Heart Institute, University of Kentucky, Lexington, Kentucky, USA

[6]Department of Cell Biology & Molecular Genetics and Maryland Pathogen Research Institute, University of Maryland, College Park, Maryland, USA

[7]Center for Bioinformatics and Computational Biology, University of Maryland, College Park, Maryland, USA

[8]Université Côte d'Azur, Centre National de la Recherche Scientifique, Institut de Pharmacologie Moléculaire et Cellulaire, Valbonne Sophia Antipolis, France

[#] These authors contributed equally to this work.

[§] These authors jointly supervised this work.

*Corresponding authors. Correspondence and request for materials should be addressed to N.K. (email: nkorotkova@uky.edu) and N.M.vS. (email: nsorge3@umcutrecht.nl).

Short title: GroP streptococcal polysaccharide modification

Keywords: streptococcus, cell wall glycopolymer, glycerol phosphate, biosynthesis, vaccine, antimicrobial mechanism

Abstract

Cell wall glycopolymers on the surface of Gram-positive bacteria are fundamental to bacterial physiology and infection biology. These structures have also gained interest as vaccine antigens, in particular for the human pathogens Group A *Streptococcus* (GAS) and *Streptococcus mutans*. Streptococcal cell wall glycopolymers are considered to be functional homologues of wall teichoic acids but surprisingly lack the biologically-relevant and characteristic anionic charge. Here we identify *gacH*, a gene of unknown function in the GAS Group A Carbohydrate (GAC) biosynthetic cluster, in two independent transposon library screens for its ability to confer resistance to zinc and susceptibility to the bactericidal enzyme human group IIA secreted phospholipase A_2. To understand the underlying mechanism of these phenotypes, we determined the structure of the extracellular domain of GacH and discover that it represents a new family of glycerol phosphate (GroP) transferases. Importantly, we demonstrate the presence of GroP in both the GAC and the homologous Serotype *c* Carbohydrate (SCC) from *S. mutans,* which is conferred by *gacH* and *sccH* products, respectively. NMR analysis of GAC released from cell wall by non-destructive methods reveals that approximately 30% of the GAC GlcNAc side-chains are modified by GroP at the C6 hydroxyl group. This previously unrecognized structural modification impacts host-pathogen interaction and has implications for vaccine design.

Graphical abstract

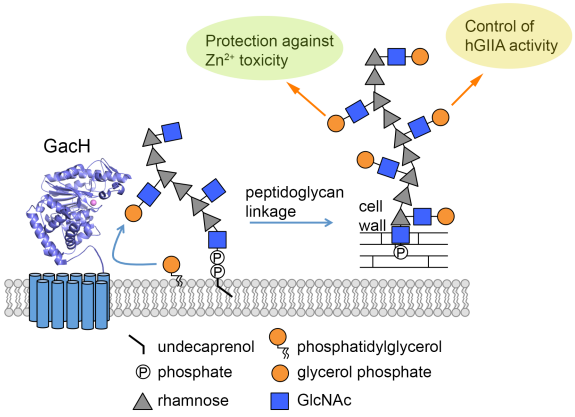

53 Gram-positive bacteria are surrounded by a thick cell wall that consists of a complex
54 network of peptidoglycan with covalently attached proteins and glycopolymers. Cell wall
55 glycopolymers comprise a large family of structurally diverse molecules, including wall teichoic
56 acid (WTA), mycobacterial arabinogalactans and capsular polysaccharides. From these, WTA is
57 perhaps the most widespread and certainly the best-studied molecule. This polyanionic,
58 phosphate-rich glycopolymer is critical for functions such as cell division, antibiotic resistance,
59 metal ion homeostasis, phage-mediated horizontal gene transfer and protection of bacteria from
60 host defense peptides and antimicrobial enzymes [1-3]. As such, these structures and their
61 biosynthetic pathways are attractive targets for therapeutic intervention, such as antibiotic
62 development and vaccine design. Interestingly, many streptococci lack expression of classical
63 WTA and instead express glycopolymers that are characterized by the presence of L-rhamnose
64 (Rha) [4]. These structures, referred to as Streptococcal Rhamnose Polysaccharides (SRPs),
65 comprise about 40-60% of the bacterial cell wall mass [5], and are historically used for serological
66 grouping of streptococci [6]. The glycopolymers of two human streptococcal pathogens, Group A
67 *Streptococcus* (GAS; *Streptococcus pyogenes*) and *Streptococcus mutans*, share a
68 characteristic [→3)α-Rha(1→2)α-Rha(1→] polyrhamnose backbone, but are distinguished
69 based on their specific glycosyl side-chain residues, i.e. *N*-acetyl-β-D-glucosamine (GlcNAc) at
70 the C3 position of Rha in GAS [7] and α-glucose (Glc) at the C2 position of Rha in *S. mutans c*
71 serotype [8]. These conserved glycopolymers, referred to as the Lancefield group A Carbohydrate
72 (GAC) and Serotype *c* specific Carbohydrate (SCC), play significant roles in the cell physiology
73 and pathogenesis of GAS and *S. mutans*, respectively. SCC-defective mutants show aberrant
74 cell morphology and division [9], increased susceptibility to certain cell wall targeting antibiotics [10],
75 defects in biofilm formation [11] and reduced ability to induce infective endocarditis compared to
76 the parental strain [12]. Biosynthesis of the rhamnan-backbone of GAC is essential for GAS
77 viability [13,14]. Moreover, GAS mutants deficient in the GAC GlcNAc side-chain are viable but
78 more susceptible to innate immune clearance by neutrophils and antimicrobial agents, resulting
79 in significant loss of virulence in animal models of GAS infection [13,15]. Importantly for both
80 pathogens, GAC and SCC have been evaluated as vaccine antigens. Indeed, immunization with
81 GAC or SCC induces opsonophagocytic antibodies that enhance killing of GAS and *S. mutans*,
82 respectively [8,16,17]. In addition, GAC has proven efficacious as a vaccine antigen through active
83 immunization in mice [16,17].

84 The GAC and SCC biosynthetic pathways are encoded by 12-gene clusters [4,13], herein
85 designated as *gacABCDEFGHIJKL* and *sccABCDEFGHMNPQ* (Fig. 1a), respectively. The first
86 seven genes in both operons are conserved in many streptococcal species and they participate

87 in polyrhamnose backbone synthesis and transport [18]. In GAS, we have demonstrated that *gacI,*
88 *gacJ, gacK* and *gacL* encode the machinery to generate and add the immunodominant GlcNAc
89 side-chain to the polyrhamnose backbone [13,19]. In *S. mutans, sccM* and *sccN* are required for
90 immunoreactivity with serotype *c*-specific antiserum suggesting a function for these genes in Glc
91 side-chain attachment to the polyrhamnose backbone [20]. In addition to these streptococcal
92 species, similar gene clusters are present in a wide variety of streptococcal, lactococcal and
93 enterococcal species, although the corresponding glycopolymer structures have not all been
94 elucidated [4].

95 Within this wider collection of species, one of the conserved genes present in the SRP
96 biosynthetic clusters, a *gacH* homologue, encodes a putative glycerol phosphate (GroP)
97 transferase of unknown function. Recently, we employed the *Krmit* GAS transposon mutant
98 library [14] and identified *gacI* and *gacH* as genes that confer sensitivity of GAS to human group
99 IIA secreted phospholipase A2 (hGIIA)
100 (https://www.biorxiv.org/content/early/2018/02/23/269779) [21], an important bactericidal protein of
101 the innate immune defense against Gram-positive pathogens [22]. Complementary, we now
102 present the data that *gacH* was the only valid hit when exposing the *Krmit* library to a lethal
103 concentration of hGIIA. Using the same transposon library, *gacH* was also identified as a gene
104 providing resistance to zinc toxicity. In pursuit of the underlying mechanisms for GacH-mediated
105 hGIIA resistance and protection against zinc toxicity, we have characterized the function of
106 GacH at the genetic, biochemical and structural level. Our study identified a previously
107 overlooked GroP modification on both GAC and SCC, and demonstrated a function of GacH
108 homologues in the transfer of GroP to SRP. GroP is attached to the GlcNAc side-chains of GAC
109 at the C6 hydroxyl group as shown by NMR analysis. These new insights into the structure,
110 biosynthesis and function of GAC and SCC justify a re-examination of the chemical structures of
111 cell wall glycopolymers in other streptococcal species. Furthermore, the discovery of GroP
112 modification of GAC and SCC offers the potential for future vaccine development and provides a
113 framework for investigation of the function of this modification in bacteria.

114 **Results**

115 **GacH homologues are required for full hGIIA bactericidal activity against GAS and**
116 ***S. mutans*.** We previously identified *gacH* in a GAS transposon library screen against the
117 bactericidal activity of hGIIA [21]. Complementary to this susceptibility screen, we also exposed
118 the *Krmit* GAS transposon library [14] to a lethal concentration of recombinant hGIIA to identify
119 resistant mutants. Only 47 colonies were recovered after exposure. Sequencing identified that
120 43% of the recovered mutants (20 out of 47) had a transposon insertion in *gacH*, and 26% in

121 *M5005_Spy_1390* (12 out of 47) (Fig. 1b). *M5005_Spy_1390* was also identified in the initial
122 susceptibility screen as an artifact due to biased transposon insertions [21] and therefore not
123 followed up further. To validate our finding for *gacH*, we generated a *gacH* deletion mutant in a
124 GAS clinical isolate of the globally-disseminated serotype M1T1 clone 5448, creating
125 5448Δ*gacH*, and complemented the mutant with *gacH* on an expression plasmid, creating
126 5448Δ*gacH:*p*gacH*. Exposure of these strains to a concentration range of hGIIA revealed that
127 deletion of *gacH* increased GAS resistance to hGIIA over 10-fold, which was restored back to
128 wild-type (WT) in 5448Δ*gacH:*p*gacH* (Fig. 1c). The *gacH*-mediated hGIIA resistance was also
129 observed in two different GAS backgrounds, 2221 (M1T1 GAS clone strain) and 5005 (clinical
130 *covS* mutant isolate of M1T1 strain) (Supplementary Fig. 1), demonstrating that the effect is
131 conserved across GAS strains of the M1T1 background and independent of CovRS status – a
132 two-component system which regulates about 15% of the genes in GAS [23].

133 Since other streptococcal species possess a genetic homologue of *gacH*, we
134 investigated whether the GacH-dependent hGIIA-resistance phenotype was conserved in
135 different streptococci. To this end, we generated a deletion mutant of the *gacH* homologue *sccH*
136 (previously known as *orf7* [20]) in serotype *c S. mutans* (SMU) strain Xc, creating SMUΔ*sccH*.
137 Deletion of *sccH* rendered *S. mutans* completely unsusceptible to the tested hGIIA
138 concentrations (Fig. 1d), which was restored to WT level by expression of *sccH* on a plasmid.
139 However, heterologous expression of *gacH* in SMUΔ*sccH* did not restore the hGIIA resistance
140 phenotype, suggesting that the enzymes might target different substrates. Taken together, our
141 data indicate that deletion of *gacH* homologues renders streptococci more resistant to the
142 bactericidal activity of hGIIA and that GacH function is species-specific. Interestingly, lack of the
143 GAC GlcNAc side-chain, by deletion of *gacI*, also increases hGIIA resistance, which is attributed
144 to reduced cell wall penetration of hGIIA [21]. These data suggest that similar to *gacI*, *gacH* might
145 participate in a tailoring modification of GAC.

146 **GacH and SccH provide protection from zinc toxicity.** Recent evidence indicates that
147 neutrophils deploy zinc poisoning as an antimicrobial strategy against GAS during
148 phagocytosis [24]. To resist Zn^{2+} toxicity, GAS expresses the zinc efflux system encoded by
149 *czcD* [24]. To search for additional GAS genes that confer resistance to zinc poisoning, we
150 performed a Tn-seq screen of the GAS *Krmit* transposon library [14] using two Zn^{2+}
151 concentrations, 10 and 20 μM, selected based on growth inhibition analysis (Supplementary Fig.
152 2a). Genomic DNA for Tn-seq analysis was collected after T2 and T3 passages (Supplementary
153 Fig. 2b). In addition to the expected importance of *czcD*, we also observed that *gacI* and *gacH*
154 transposon insertions were significantly reduced in the library (P-value of <0.05) after growth

155 with 20 μM Zn^{2+} in both T2 and T3 passages compared to untreated controls indicating that the
156 genes provide resistance against Zn^{2+} toxicity (Fig. 2a-d).

157 To confirm that *gacI* and *gacH* are required for GAS resistance to Zn^{2+}, we grew
158 5448Δ*gacH* and 5448Δ*gacI* [13] on THY agar supplied with different concentrations of Zn^{2+} (Fig.
159 2e and 2f). The growth of both mutants was reduced in THY supplied with 1.25 mM Zn^{2+}.
160 Expression of full-length *gacH* in 5448Δ*gacH,* and *gacI* in 5448Δ*gacI* fully complemented the
161 growth phenotypes of the mutants. To investigate whether this was a conserved function for
162 *gacH* homologues, we extended our experiments to *S. mutans*. Similar to the GAS *gacH*
163 deletion mutant, SMUΔ*sccH* was more sensitive to Zn^{2+}, in comparison to the parental strain
164 and the phenotype can only be restored by *sccH* but not *gacH* (Supplementary Fig. 3). Hence,
165 our results provide strong evidence that the unknown functions of GacH and SccH are important
166 for protection of streptococci from Zn^{2+} toxicity.

167 **GacH structure.** GacH is predicted to contain eleven transmembrane segments in its N-
168 terminal domain, and a C-terminal extracellular domain (eGacH), that is likely to perform the
169 enzymatic function. To gain insight into GacH function, the extracellular domain of GacH
170 (eGacH) was expressed and purified from *E. coli* and its crystal structure was determined in apo
171 form (PDB ID 5U9Z) at 2.0 Å resolution (Fig. 3a). Additionally, to test the hypothesis that GacH
172 is a GroP transferase, we solved the structure of eGacH in complex with GroP (PDB ID 6DGM)
173 at 1.49 Å resolution (Fig. 3c). The apo- and GroP-containing eGacH structures belong to
174 different crystal forms, with two molecules in the asymmetric unit. Analysis of the dimer interface
175 and other crystal contacts revealed that the dimer interface has the largest surface of all the
176 crystal contacts (1809 and 1894 $Å^2$ in the two crystal forms). However, it is scored below the
177 stable complex formation criteria, and recombinant eGacH behaves as a monomer in solution.
178 This does not exclude a possibility of a dimer formation in the context of the full-length GacH.
179 The structures of the apo- and GroP-bound eGacH monomers are very similar with root mean
180 square deviation of 0.3 Å for 380 superimposed $C\alpha$ atoms, as well as between the non-
181 crystallographic copies.

182 eGacH has an α/β core structure that is similar of the sulfatase protein family, with the
183 closest similarity to lipoteichoic acid (LTA) synthase LtaS [25,26] and LTA primase LtaP [27]
184 (Supplementary Table 1). LtaS and LtaP are GroP transferases that participate in biosynthesis
185 of LTA, a crucial cell envelope constituent of Gram-positive bacteria. LTA is an anionic polymer
186 consisting of a polyglycerol-phosphate backbone linked to a glycolipid membrane anchor [28]. The
187 catalytic site of GacH contained a Mn^{2+} ion coordinated by residues E488, T530, D711 and
188 H712, equivalent to residues E255, T300, D475 and H476 of *Staphylococcus aureus* LtaS (Fig.

189 3c, Supplementary Fig. 4d and 5). The structure of GacH in complex with GroP revealed the
190 position of the ligand in the active site with the phosphoryl group oriented towards the Mn^{2+} ion,
191 and coordinated by residues G529, T530 and H650 (Fig. 3c). The glycerol 2- and 3-hydroxyl
192 groups form hydrogen bonds with side-chains of residues R589, H580 and N586. The positions
193 of GroP and coordinating residues are similar in eGacH and *S. aureus* LtaS structures. For
194 example, the glycerol moiety forms hydrogen bonds with residues H580 and R589 in GacH and
195 equivalent residues H347 and R356 in *S. aureus* LtaS (Fig. 3c and Supplementary Fig. 4d) [25].
196 Thus, the structure of GacH in complex with GroP is consistent with the idea that GacH and
197 LtaS use related catalytic mechanisms of GroP transfer to substrates.

198 **GacH homologues form a distinct clade of GroP transferases.** Taking into
199 consideration GacH structural homology to LtaS, we examined the distribution of the GacH
200 family of proteins throughout the bacterial kingdom and compared the evolutionary relatedness
201 of GacH with LtaS. Interestingly, with a few exceptions, GacH homologues were found
202 predominantly in streptococcal species (Fig. 3d, Supplementary Fig. 4e). In contrast to GacH
203 that contains eleven predicted transmembrane segments, LtaS is composed of an N-terminal
204 domain with five transmembrane helices [25-27,29]. Based on just the extracellular domains of the
205 proteins, GacH and LtaS-related proteins are grouped in separate clades on a phylogenetic
206 tree, suggesting that the proteins may fulfill distinct functions in bacteria by transferring GroP to
207 different substrates (Fig. 3d).

208 **GacH homologues decorate respective SRPs with GroP**. The genetic, bioinformatic
209 and structural evidence presented in the preceding sections strongly suggest that *gacH* and
210 *sccH* encode novel GroP transferases of unknown function in GAS and *S. mutans*
211 (Supplementary Fig. 6). The presence of these genes in the GAC and SCC biosynthetic clusters
212 implies that they may participate in polysaccharide synthesis in a previously undefined manner.
213 To investigate the possibility that GacH and SccH function in the modification of the respective
214 SRPs with GroP, we enzymatically released SRP from purified cell walls (free of LTA, lipids,
215 proteins and nucleic acids) from GAS 5005, *S. mutans* WT, and corresponding *gacH* and *sccH*
216 deletion strains by treatment with peptidoglycan hydrolases (as described in Methods).
217 Subsequently, the enriched polysaccharide preparations were analyzed for glycerol and
218 phosphate. Hydrolysis with HCl (2 N HCl, 100 °C, 1 hr) released a significant amount of glycerol
219 from GAC and SCC isolated from WT bacterial strains (Fig. 4a, b, and Supplementary Fig. 7).
220 Furthermore, we detected high levels of inorganic phosphate after incubation of these acid-
221 treated samples with alkaline phosphatase (Fig. 4a, b). Of note, the treatment of intact GAC and
222 SCC with alkaline phosphatase alone did not release detectable levels of phosphate

223 (Supplementary Fig. 7), indicating that the phosphoryl moiety is present as a phosphodiester,
224 presumably as GroP. In contrast to WT GAC and SCC, the SRPs isolated from the *gacH* and
225 *sccH* mutants (5005Δ*gacH* and SMUΔ*sccH*, respectively) contained a significantly reduced
226 amount of GroP (Fig. 4a, b). Genomic complementation of 5005Δ*gacH* phenotype by
227 expression of *gacH* on the mutant chromosome restored the WT levels of GroP in GAC (Fig.
228 4a). Similarly, complementation of SMUΔ*sccH* with plasmid-expressed *sccH* restored GroP
229 incorporation of the mutant to the level of the parental strain (Fig. 4b). In contrast but in
230 accordance with our functional data, expression of *gacH* did not restore the GroP levels in SCC
231 of SMUΔ*sccH* (Fig. 4b). Importantly, analysis of the glycosyl composition of cell walls purified
232 from the GAS and *S. mutans* strains demonstrated that the absence of GacH and SccH did not
233 affect the Rha/GlcNAc and Rha/Glc ratios, respectively (Supplementary Fig. 8). Since the
234 differences in GroP content for 5005Δ*gacH* and SMUΔ*sccH* were not due to changes in the
235 composition of GAC and SCC, our results are consistent with a role for SccH and GacH in
236 modification of SRPs by GroP.

237 Both structurally and functionally, we can only complement the SMUΔ*sccH* mutant by
238 expression of the native *sccH*, suggesting that the site of GroP attachment to SRPs might
239 involve the species-specific side-chains (Glc vs. GlcNAc), rather than the identical
240 polyrhamnose backbone. Consistent with this hypothesis, the glycerol and phosphate contents
241 in the GAC isolated from two GlcNAc-deficient mutants, 5005Δ*gacL* and 5005Δ*gacI* [19] were
242 significantly reduced, similarly to 5005Δ*gacH* (Fig. 4c, d).

243 To prepare bacterial polysaccharide for more detailed analysis, GAC was released from
244 isolated cell walls by peptidoglycan hydrolase treatment and partially purified by a combination
245 of size exclusion chromatography (SEC) and ion-exchange chromatography (Fig. 4e,
246 Supplementary Fig. 9a). Fractions from both chromatography analyses were assayed for Rha
247 and total phosphate. The majority of the rhamnose- and phosphate-containing material was
248 bound to the ion-exchange column and eluted as a single coincident peak (Fig. 4e). Similarly
249 prepared GAC purified from 5005Δ*gacH* did not bind to the column (Supplementary Fig. 9b).
250 Interestingly, the GAC from 5005Δ*gacH* does appear to contain a small amount of phosphate,
251 although its phosphate content is much lower than the GAC isolated from the WT strain. This
252 data directly supports the conclusion that GAC is modified with GroP donated by GacH.

253 **Identification of the enantiomeric form of GroP associated with GAC.** LTA is formed
254 by the sequential addition of *sn*-Gro-1-P groups transferred by LtaS from the head group of the
255 membrane lipid phosphatidylglycerol [30,31]. In contrast, the *Bacillus subtilis* poly-GroP backbone
256 of WTA consists of *sn*-Gro-3-P repeats that are synthesized on the cytoplasmic surface of the

257 plasma membrane from CDP-glycerol before export to the periplasm and attachment to the cell
258 wall [1]. Since GacH and SccH are LtaS homologues, it is possible that the incorporated GroP is
259 derived from phosphatidylglycerol yielding *sn*-Gro-1-P residues. To test this hypothesis, GroP
260 was liberated from purified GAC by alkaline hydrolysis and separated from the polysaccharide
261 by SEC. As explained in detail by Kennedy *et al* [32] for GroP-modified membrane
262 oligosaccharides from *E. coli*, if GAC is modified by *sn*-Gro-1-P, alkaline hydrolysis of the
263 phosphodiester bond should result in the formation of two cyclic intermediate compounds, Gro-
264 1-cyclic phosphate and Gro-2-cyclic phosphate which further break up to a mixture of *sn*-Gro-1-
265 P and Gro-2-P [32]. If GAC is modified by *sn*-Gro-3-P, alkaline hydrolysis would yield a mixture of
266 *sn*-Gro-3-P and Gro-2-P [32], whereas a phosphodiester of Gro-2-P would give a mixture of all
267 three phosphates [32]. Following alkaline hydrolysis the bulk of the carbohydrate still elutes in the
268 void volume of the SEC column (Supplementary Fig. 10). However, the phosphate-containing
269 fractions corresponding to the hydrolyzed GroP now elute in the inclusion volume
270 (Supplementary Fig. 10). The enantiomeric composition of the GroP preparation was
271 determined using a combination of LC-MS and an enzymatic method (see below). LC-MS
272 revealed the presence of two GroP isomers, of approximately equal proportions, with LC
273 retention times and major high molecular weight ions consistent with standard *sn*-Gro-1-P and
274 Gro-2-P (Fig. 4f–4h, Supplementary Fig. 11). To resolve whether *sn*-Gro-3-P or *sn*-Gro-1-P is
275 the substituent, the recovered GroP was characterized further by enzymatic analysis using a
276 commercially available *sn*-Gro-3-P assay kit. Under reaction conditions in which 500 pmol of *sn*-
277 Gro-3-P produced a robust enzymatic signal, incubation with either 500 pmol of *sn*-Gro-1-P or
278 500 pmol of the unknown Gro-P, recovered following alkaline hydrolysis, resulted in negligible
279 activity (Supplementary Fig. 12). When a mixture containing 500 pmol of standard *sn*-Gro-3-P,
280 and an equal amount of either *sn*-Gro-1-P or the unknown mixture of Gro-P isomers were
281 tested, 85.8% and 90.0% of the activity detected with 500 pmol *sn*-Gro-3-P, alone, was found,
282 demonstrating that the negative result using the unknown mixture, by itself, was not due to the
283 presence of an unknown inhibitory compound in the GroP preparation. Taken together, our
284 results indicate that GacH decorates GAC with *sn*-Gro-1-P, which is most probably derived from
285 phosphatidylglycerol.

286 **NMR spectroscopy confirms the presence of GroP at the C6 hydroxyl group of**
287 **GlcNAc side-chains.** To unambiguously prove the incorporation of GroP in GAC, the
288 polysaccharide isolated from WT GAS as described above was employed for NMR analysis
289 (Fig. 5 a-g). ^{1}H and ^{13}C NMR spectra of GAC confirmed the presence of Rha and GlcNAc in a
290 1.7:1 ratio as determined by a chemical analysis of its sugar components. Although the material

291 was heterogeneous, initial analysis revealed that it would be possible to analyze the purified
292 GAC at different levels of detail. The major component identifiable at the highest level of
293 intensity in a multiplicity-edited ^{1}H,^{13}C-HSQC NMR spectrum (Supplementary Fig. 13), acquired
294 by non-uniform sampling at the 25% level of coverage facilitating enhanced resolution to resolve
295 spectral overlap [33], revealed the ^{1}H NMR chemical shifts in agreement with the following
296 structure →3)-α-L-Rha*p*-(1→2)[β-D-Glc*p*NAc-(1→3)]-α-L-Rha*p*-(1→ as its repeating unit; [7] the
297 $^{1}J_{HC}$-based correlations facilitated identification of the resonances of the proton-carrying ^{13}C
298 nuclei.

299 An array of 2D NMR experiments including ^{1}H,^{1}H-TOCSY, ^{1}H,^{1}H-NOESY, ^{1}H,^{13}C-HMBC
300 and ^{1}H,^{13}C-HSQC-TOCSY led to the ^{1}H and ^{13}C NMR chemical shift assignments
301 (Supplementary Table 2) and confirmed the structure of the trisaccharide repeating unit. A
302 number of additional cross-peaks were visible at the second intensity level of the ^{1}H,^{13}C-HSQC
303 spectrum, particularly in the spectral region of methylene groups, e.g. hydroxymethyl groups of
304 hexopyranses [34]. Besides the resonances from the hydroxymethyl group of the β-D-Glc*p*NAc
305 residue at δ_H 3.78 and 3.94 correlated with a signal at δ_C 61.8, three more ^{13}C signals together
306 with corresponding ^{1}H resonances were present at δ_C 63.1, 65.4 and 67.3 (Fig. 5a), readily
307 identified from the multiplicity-editing applied in the experiment. In the ^{13}C NMR spectrum two
308 resonances at δ_C 67.3 and 71.6 were conspicuous in that they were split by 5.6 and 7.6 Hz,
309 respectively. A ^{13}C resonance observed as a doublet in this manner suggests scalar coupling to
310 the NMR active nucleus ^{31}P [35] and acquisition of a ^{31}P NMR spectrum on GAC showed a
311 prominent resonance at δ_P 1.2. The ^{1}H,^{1}H-TOCSY NMR spectrum at the second intensity level
312 revealed chemical shift displacements in the region for anomeric resonances (Supplementary
313 Fig. 14), and in the ^{1}H,^{13}C-HSQC-TOCSY spectrum two correlations from the anomeric proton
314 resonance at δ_H ~4.76 were observed to δ_C 61.8 (C6 in β-D-Glc*p*NAc) and to δ_C 65.4 (Fig. 5b).
315 Employing a ^{1}H,^{31}P-HMBC experiment revealed correlations to protons of the latter ^{13}C at δ_H
316 4.10 and 4.19 as well as to δ_H 3.91 and 3.96, the ^{13}C nucleus of which resonates at δ_C 67.3 (Fig.
317 5c). Moreover, a ^{1}H,^{31}P-hetero-TOCSY experiment showed in addition to the just described
318 proton correlations further correlations to δ_H 3.59, 3.64 and 3.70 (Fig. 5d). Using the arsenal of
319 2D NMR experiments the resonances at the second level deviating from the parent structure
320 were assigned (Supplementary Table 2). Thus, the GAC is partially substituted by a GroP
321 residue at O6 of the side-chain β-D-Glc*p*NAc residue; based on integration of the cross-peaks
322 for the anomeric resonances in the ^{1}H,^{13}C-HSQC NMR spectrum, the GAC preparation carries
323 GroP groups to ~30 % of the GlcNAc residues. To validate the above results, a triple-resonance
324 ^{1}H,^{13}C,^{31}P NMR experiment based on through-bond $^{1}J_{HC}$ as well as $^{2}J_{CP}$ and $^{3}J_{CP}$ correlations [36]

was carried out. The 3D NMR experiment revealed the ^{1}H NMR chemical shifts of H5' and the two H6' protons of the β-D-Glc*p*NAc residue, as well as the two H1' protons and H2' of the Gro residue all correlated to ^{13}C nuclei (Fig. 5e). The ^{13}C NMR chemical shifts of C5' and C6' of the β-D-Glc*p*NAc residue as well as C1' and C2' of the Gro residue all correlated to the ^{31}P nucleus (Fig. 5f), and the above protons correlated to the ^{31}P nucleus (Fig. 5g). Taking into considerations the GacH-mediated mechanism of GAC modification by GroP as well as the biochemical experiments carried out herein, the substituent at O6 of β-D-Glc*p*NAc is an *sn*-Gro-1-P group (Fig. 5h).

Discussion

In Gram-positive bacteria, the common theme of most peptidoglycan-attached carbohydrate-based polymers is the presence of negatively charged groups in the repeating units [3]. For example, canonical and non-canonical WTAs and Group B carbohydrate of *Streptococcus agalactiae* contain phosphodiester groups in the repeating units, peptidoglycan of *B. subtilis* grown in phosphate limiting conditions is decorated with a teichuronic acid containing glucuronic acid, and secondary cell wall carbohydrates of *Bacillus anthracis* are modified with pyruvyl groups [2-4]. In bacteria lacking WTA such as the human pathogens GAS and *S. mutans*, it has been proposed that other polyanionic structures, such as LTA, fulfill similar functions during the bacterial cell cycle [4,37]. Previous detailed studies using immunochemical methods, composition and linkage analyses and NMR methods deduced chemical structures of peptidoglycan-attached SRPs from both streptococcal species [7,8,38-42], but none identified anionic groups in these structures, except one overlooked study in which the presence of glycerol and phosphate in GAC has been detected [43]. However, it was proposed that this GroP is part of the phosphodiester linkage connecting GAC to the N-acetylmuramic acid of peptidoglycan [43]. Similarly, a number of reports identified substantial concentrations of phosphate in SRPs isolated from *Streptococcus sanguis*, *Streptococcus gallolyticus*, *Streptococcus dysgalactiae*, *Streptococcus sobrinus* serotype *d* and *S. mutans* serotype *f* [30,42,44,45]. These phosphate-rich polymers were either disregarded as contamination with LTA [30], or further analyzed using ^{1}H NMR or ^{13}C NMR methods [7,8,40-42,46,47] that do not directly detect phosphoryl moieties in polysaccharides. With our report, we unambiguously confirm that SRPs of GAS and *S. mutans* are in fact polyanionic glycopolymers through decoration of their respective glycan side-chains with GroP (Fig. 5i).

We identified and structurally characterized a new family member of GroP transferase enzyme, GacH, which is required for GAC modification with GroP in GAS. GacH homologues are present in the SRP biosynthetic loci of many streptococci suggesting that a large proportion

359 of streptococcal species produce SRPs where glycosyl side-chains are decorated with GroP
360 similar to our observations for *S. mutans*. GacH is predicted to be an extracellular protein
361 anchored in the cytoplasmic membrane. It belongs to the alkaline phosphatase superfamily of
362 which two GroP transferases involved in LTA synthesis, LtaS and LtaP, have been
363 biochemically and structurally characterized to date [25-27,29]. LtaS and LtaP are membrane
364 proteins that use the membrane lipid phosphatidylglycerol as the GroP donor for the transfer
365 reaction [48,49]. Our structural analysis of GacH in complex with GroP indicates that the enzyme
366 uses the catalytic T530 residue to participate in the formation of a GroP-enzyme intermediate.
367 This corresponds to the structure of LtaS, where the GroP molecule is complexed in the active
368 site in which a threonine residue functions as a nucleophile in phosphatidylglycerol
369 hydrolysis [25-27]. The observation that the GroP in GAC is the *sn*-Gro-1-P enantiomer, strongly
370 suggests that GacH uses phosphatidylglycerol as its donor substrate, similar to LtaS (Fig. 5i).
371 Thus our data propose a catalytic mechanism in which GacH binds phosphatidylglycerol and
372 T530 functions as a catalytic nucleophile to attack the GroP head group and cleave the
373 phosphodiester bond. Diacylglycerol is released, leaving a covalent GroP-T530 intermediate.
374 Next, the C6 hydroxyl group of the GAC GlcNAc target is deprotonated and then attacks the
375 GroP-T530 enzyme, forming the GroP-GlcNAc product and returning the enzyme to the apo
376 state.

377 In Gram-positive bacteria, the tailoring modification of WTA and LTA with D-alanine
378 provides resistance against antibiotics, cationic antimicrobial peptides and small bactericidal
379 enzymes including hGIIA, and promotes Mg^{2+} ion scavenging [1-3]. It has been assumed that
380 incorporation of positively charged D-alanine into teichoic acids decrease negative bacterial
381 surface charge resulting in reduced initial binding of cationic antimicrobial peptides to the
382 bacterial surface due to ionic repulsion [50,51]. Our study demonstrates that addition of the
383 negatively charged GroP group to SRPs protects streptococci from zinc toxicity but also renders
384 bacteria more sensitive to hGIIA activity. A large body of published evidence indicates that
385 phagocytic cells utilize Zn^{2+} intoxication to suppress the intracellular survival of bacteria [52]. The
386 mechanism of microbial susceptibility to zinc toxicity is mediated by extracellular competition of
387 Zn^{2+} for Mn^{2+} transport and thereby mediating toxicity by impairing Mn^{2+} acquisition [53].
388 Accordingly, the phenotypes of our mutants deficient in the GroP modifications and the GlcNAc
389 side-chains could be explained either by "trapping" of Zn^{2+} in the WT cell wall as a consequence
390 of zinc binding to negatively-charged GroP, or the increased Mn^{2+}-binding capacity of GroP-
391 modified bacterial cell wall which has been proposed to act as the conduit for the trafficking of
392 mono- and divalent cations to the membrane [2].

393 Charge-dependent mechanisms are likely also underlying the increased hGIIA
394 susceptibility of GAS and *S. mutans* expressing the GroP-modified SRPs. hGIIA is a highly
395 cationic enzyme that catalyzes the hydrolysis of bacterial phosphatidylglycerol [54-56], ultimately
396 leading to bacterial death. It has been suggested that traversal of this bactericidal enzyme
397 across the Gram-positive cell wall to reach the plasma membrane is charge dependent because
398 the absence of positively-charged D-alanine modifications in LTA and WTA severely
399 compromises *S. aureus* survival when challenged with hGIIA [56,57]. This phenotype was
400 attributed to increased binding of hGIIA to the cell surface or modified permeability of the cell
401 envelope. Similarly, the GacH/SccH-dependent GroP modifications on SRPs are required for
402 hGIIA to exert its bactericidal effect against GAS and *S. mutans*, respectively. We have
403 previously demonstrated that loss of the GlcNAc GAC side-chain strongly hampers trafficking of
404 hGIIA through the GAS cell wall, with a minor contribution of reduced hGIIA binding to the cell
405 surface [21]. Since GroP-modifications were also lost in the GlcNAc side-chain deficient mutant,
406 5448Δ*gacI*, described in this study, we now assume that the mechanisms of the hGIIA-
407 dependent phenotype are similar in the *gacI* and *gacH* mutants.
408 Another very important aspect of our study is the identification of a novel, potentially
409 antigenic, epitope on the surface of streptococcal bacteria. GAS is a major human pathogen,
410 and is associated with numerous diseases ranging from minor skin and throat infections such as
411 impetigo and pharyngitis to life-threatening invasive diseases such as scarlet fever,
412 streptococcal toxic syndrome and rapidly progressing deep-tissue infections, necrotizing fasciitis
413 (i.e. the “flesh eating disease”), cellulitis and erysipelas [58]. GAS infections are also responsible
414 for post-infectious autoimmune syndrome, rheumatic fever (RF) and its sequelae, rheumatic
415 heart disease (RHD) [58]. Invasive GAS infections are difficult to treat with antibiotics and a GAS
416 vaccine is urgently needed to combat this neglected disease. GAC is an attractive candidate for
417 GAS vaccine due to its conserved expression in all GAS serotypes and the absence of the
418 constitutive component of GAC, Rha, in humans [16,17]. However, it has been proposed that the
419 GAC GlcNAc side-chain can elicit the cross-reactive antibodies relevant to the pathogenesis of
420 RF and RHD [59-61]. Moreover, persistence of anti-GAC and anti-GlcNAc antibodies is a marker of
421 poor prognosis in RHD [60,62]. These clinical associations and the lack of understanding of the
422 pathogenesis of GAS post-infectious RHD have hampered progress in the development of
423 GAC-based vaccines against GAS. However, the GAC GlcNAc decorated with GroP might be a
424 feasible candidate for GAS vaccine development because modified GlcNAc represents a unique
425 epitope, that is absent from human tissues. Thus, our study has implications for design of a safe
426 and effective vaccine against this important human pathogen for which a vaccine is not yet

427 available. Finally, our work provides a framework for structure-function investigations of cell wall
428 modifications in streptococci.
429
430 **Methods**
431 **Bacterial strains, growth conditions and media**
432 All plasmids, strains and primers used in this study are listed in Supplementary Tables 3 and 4.
433 Streptococcal strains used in this study were the M1-serotype GAS strains, 5448 [14], 2221 [63] and
434 5005 [63], and *c* serotype *S. mutans* Xc [64]. GAS and *S. mutans* strains were grown in Todd-Hewitt
435 broth supplemented with 1% yeast extract (THY) without aeration at 37 °C. *S. mutans* plates
436 were grown with 5% CO_2. For hGIIA-mediated killing experiments *S. mutans* strains were grown
437 in Todd-Hewitt broth without yeast extract and with 5% CO_2. *E. coli* strains were grown in
438 Lysogeny Broth (LB) medium or on LB agar plates at 37 °C. When required, antibiotics were
439 included at the following concentrations: ampicillin at 100 μg/mL for *E. coli*; streptomycin at 100
440 μg/mL for *E. coli*; erythromycin (Erm) at 500 μg/mL for *E. coli* and 5 μg/mL for GAS and *S.*
441 *mutans*; chloramphenicol (CAT) at 10 μg/mL for *E. coli* and 2 μg/mL for GAS and *S. mutans*;
442 spectinomycin at 200 μg/mL for *E. coli*, 100 μg/mL for GAS and 500 μg/mL for *S. mutans*.
443 To identify GAS genes providing resistance against zinc toxicity, we used chemically
444 defined medium based on the formulation of RPMI 1640 medium [65], which mirrors the amino
445 acid composition of the van de Rijn and Kessler formulation [66]. This RPMI 1640 (without
446 glucose) (Gibco) is supplemented with nucleobases guanine, adenine and uracil at a
447 concentration of 25 μg/mL each, as well as D-glucose at a final concentration of 0.5% w/v and
448 HEPES at 50 mM. Necessary vitamins for GAS growth are provided by 100X BME Vitamins
449 (Sigma B6891). The final solution (mRPMI) is pH 7.4 and capable of supporting GAS growth
450 without additional supplements.
451 **Genetic manipulations**
452 *DNA techniques:* Plasmids were transformed into GAS and *S. mutans* by electroporation or
453 natural transformation as described previously [9,67]. Chromosomal DNA was purified from GAS
454 and *S. mutans* as described [68]. All constructs were confirmed by sequencing analysis (Eurofins
455 MWG Operon and Macrogen).
456 *Genetic manipulation of GAS 5005 and 2221:* For construction of the 5005Δ*gacH* and
457 2221Δ*gacH* strains, 5005 chromosomal DNA was used as a template for amplification of two
458 DNA fragments using two primers pairs: 5005-f/gacHdel-r and gacHdel-f/5005-r. Primer
459 gacHdel-f is complementary to primer gacHdel-r. The two gel-purified PCR products containing
460 complementary ends were mixed and amplified using a PCR overlap method [69] with primer pair

461 5005-f/5005-r to create the deletion of *gacH*. The PCR product was digested with BamHI and
462 XhoI and ligated into BamHI/SalI-digested plasmid pBBL740. The integrational plasmid
463 pBBL740 does not have a replication origin that is functional in GAS, so the plasmid can be
464 maintained only by integrating into the GAS chromosome through homologous recombination.
465 The plasmid was designated pBBL740Δ*gacH*. The resulting plasmid was transformed into 5005
466 and 2221, and CAT resistant colonies were selected on THY agar plates. Five randomly
467 selected colonies, that had the first crossover, were grown in liquid THY without CAT for ≥5
468 serial passages. Several potential double crossover mutants were selected as previously
469 described [70]. The deletion in each mutant was confirmed by PCR sequencing of the loci.
470 To construct the plasmid for *in cis* complementation of the 5005Δ*gacH* mutant, 5005
471 chromosomal DNA was used as a template for amplification of a wild-type copy of *gacH* using
472 the primer pair 5005-f/5005-r. The PCR products were digested with BamHI and XhoI, and
473 cloned in pBBL740 previously digested with the respective enzymes. The plasmid was
474 designated pBBL740*gacH*. The plasmid was transformed into the 5005Δ*gacH* strain, and CAT
475 resistant colonies were selected on THY agar plates. Double crossover mutants were selected
476 as described above. Selected mutants were confirmed by PCR sequencing, yielding strain
477 *5005ΔgacH:gacH.*
478 *Genetic manipulation of GAS 5448:* For construction of the 5448Δ*gacH* strains, GAS 5448
479 chromosomal DNA was used to amplify up and downstream regions flanking *gacH* using the
480 following primer pairs: 5448-f/5448CAT-r and 5448CAT-f/5448-r. Primers 5448CAT-f and
481 5448CAT-r contain 25 bp extensions complementary to the CAT resistance cassette. Up- and
482 downstream were fused to the CAT cassette using 5448-f/5448-r, digested with XhoI and HindIII
483 and ligated into XhoI/HindIII-digested plasmid pHY304, yielding plasmid pHY304Δ*gacH*. After
484 transformation in electrocompetent GAS 5448, transformed colonies were selected in THY
485 containing Erm at 30 °C. After confirmation by PCR, transformed colonies were shifted to the
486 non-permissive temperature of 37 °C to allow plasmid integration. Serial passage at 30 °C in the
487 absence of antibiotic enabled occurrence of double cross-over events, yielding 5448Δ*gacH*,
488 which were identified by screening for Erm sensitivity and CAT resistance. Deletion of *gacH* was
489 confirmed by PCR.
490 To complement 5448Δ*gacH*, we created an expression plasmid p*gacH*_erm. *GacH* was
491 amplified from GAS 5448 chromosomal DNA using primer pair gacH-EcoRI-f/gacH-BglII-r,
492 digested using EcoRI/BglII, and ligated into EcoRI/BglII-digested pDCerm. p*gacH*_erm was
493 transformed into the electrocompetent 5448Δ*gacH* and selected for Erm resistance on THY
494 agar plates. Transformation was confirmed by PCR, yielding strain *5448ΔgacH:*p*gacH*.

495 *Genetic manipulation of S. mutans* Xc. For construction of the *sccH* deletion mutant
496 (SMUΔ*sccH*), *S. mutans* Xc chromosomal DNA was used to amplify up and downstream
497 regions flanking using the following primer pairs: sccH-f/sccH-erm-r and sccH-erm-f /sccH-r.
498 Primers sccH-erm-f and sccH-erm-r contain 25 bp extensions complementary to the Erm
499 resistance cassette. Up and downstream PCR fragments were mixed with the Erm cassette and
500 amplified as a single PCR fragment using primer pair sccH-f/sccH-r. The *sccH* knockout
501 construct was transformed into *S. mutans* as described previously [9]. Erm resistant single
502 colonies were picked and checked for deletion of *sccH* and integration of Erm cassette by PCR
503 using primer pair: sccH-c-f/sccH-c-r, resulting in SMUΔ*sccH*. For complementation, *sccH* and
504 *gacH* were amplified from *S. mutans Xc* and GAS 5448 chromosomal DNA, respectively, using
505 primer pairs sccH-EcoRI-f/sccH-BglII-r and gacH-EcoRI-f/gacH-BglII-r. The PCR products were
506 digested with EcoRI/BglII, and ligated into EcoRI/BglII-digested pDC123 vector, yielding p*sccH*
507 and p*gacH*_cm, respectively. The plasmids were transformed into SMUΔ*sccH* as described [9].
508 CAT resistant single colonies were picked and checked for presence of p*sccH* or p*gacH*_cm by
509 PCR, yielding strains SMUΔ*sccH:*p*sccH* and SMUΔ*sccH:*p*gacH*, respectively.
510 *Construction of the plasmids for* E. coli *expression of gacH:* To create a vector for expression of
511 extracellular domain of GacH, the gene was amplified from 5005 chromosomal DNA using the
512 primer pair gacH-NcoI-f and gacH-XhoI-r. The PCR product was digested with NcoI and XhoI,
513 and ligated into NcoI/XhoI-digested pET-NT vector. The resultant plasmid, pETGacH, contained
514 *gacH* fused at the N-terminus with a His-tag followed by a TEV protease recognition site.
515 **Protein expression and purification**
516 For expression and purification of eGacH, *E. coli* Rosetta (DE3) cells carrying the respective
517 plasmid were grown to an OD_{600} of 0.4-0.6 and induced with 0.25 mM isopropyl β-D-1-
518 thiogalactopyranoside (IPTG) at 18 °C for approximately 16 hrs. The cells were lysed in 20 mM
519 Tris-HCl pH 7.5, 300 mM NaCl with two passes through a microfluidizer cell disrupter. The
520 soluble fractions were purified by Ni-NTA chromatography with washes of 20 mM Tris-HCl pH
521 7.5, 300 mM NaCl and 20 mM Tris-HCl pH 7.5, 300 mM NaCl, 10 mM imidazole, and elution
522 with 20 mM Tris-HCl pH 7.5, 300 mM NaCl, 250 mM imidazole. The eluate was dialyzed into 20
523 mM Tris-HCl pH 7.5, 300 mM NaCl in the presence of TEV protease (1 mg per 20 mg of
524 protein). The dialyzed sample was reapplied to a Ni-NTA column equilibrated in 20 mM Tris-HCl
525 pH 7.5, 300 mM NaCl to remove the cleaved His-tag and any uncleaved protein from the
526 sample. eGacH was further purified by size exclusion chromatography (SEC) on a Superdex
527 200 column in 20 mM HEPES pH 7.5, 100 mM NaCl, with monitoring for protein elution at 280

528 nm. Fractions collected during elution from the column were analyzed for purity by SDS-PAGE
529 and concentrated to approximately 10 mg/mL.
530 For expression of seleno-methionine labeled eGacH, *E. coli* Rosetta (DE3) carrying
531 eGacH was grown in LB at 37 °C until an optical density at 600 nm of approximately 0.5 was
532 obtained. The bacteria were centrifuged and resuspended in M9 minimal media supplemented
533 with seleno-methionine. After a significant increase in optical density, protein expression was
534 induced with 0.25 mM IPTG, and the cultures were grown at 16 °C for approximately 16 hrs.
535 Seleno-methionine labeled eGacH was purified as described above.
536 **Crystallization, data collection and structure solution**
537 eGacH crystallization conditions were initially screened using the JCSG Suites I–IV screens
538 (Qiagen) at a protein concentration of 9 mg/mL by hanging drop vapor diffusion method.
539 Crystals of Se-Met-substituted eGacH were grown in 0.1 M HEPES pH 7.5, 10% PEG8000, 8%
540 ethylene glycol. Crystals were transferred into crystallization solution supplemented with 20%
541 ethylene glycol and flash frozen in liquid nitrogen. The data were collected at APS 22-ID at a
542 wavelength of 0.9793 Å. Crystals of GroP•eGacH complex were obtained using crystallization
543 solution containing 0.2 M calcium acetate, 0.1 M MES pH 6.0, 20% PEG8000. *sn*-glycerol-1-
544 phosphate (Sigma Aldrich) was mixed with eGacH at 10 mM prior to crystallization. Initial
545 crystals of GroP•eGacH complex belonged to the same crystal form as apo GacH, however,
546 crystals of different morphology grew epitaxially after several days. These crystals displayed
547 better diffraction and were used for structure determination of GroP•eGacH complex. Crystals
548 were cryoprotected in crystallization solution supplemented with 10 mM *sn*-glycerol-1-phosphate
549 and 20% ethylene glycol and vitrified in liquid nitrogen. The data were collected at SSRL BL9-2
550 at a wavelength of 0.97946 Å.
551 All data were processed and scaled using *XDS* and *XSCALE* [71]. The structure of eGacH
552 was solved by Se single-wavelength anomalous diffraction method. Se atoms positions were
553 determined using HySS module in *PHENIX* [72,73]. The structure was solved using AutoSol wizard
554 in *PHENIX* [74]. The model was completed using *Coot* [75] and refined using *phenix.refine* [76]. The
555 final structure has two eGacH molecules in the asymmetric unit containing residues 444–822.
556 The structure of GroP•eGacH complex was solved by molecular replacement using
557 *Phaser* [77] and the dimer of apo eGacH as a search model. The model was adjusted using *Coot*
558 and refined using *phenix.refine*. Difference electron density corresponding to GroP molecules
559 was readily identified after refinement. GroP molecules were modeled using *Coot*. The
560 geometric restraints for GroP were generated using Grade Web Server
561 (http://grade.globalphasing.org) (Global Phasing). The last several rounds of refinement were

562 performed using 19 translation/libration/screw (TLS) groups, which were identified by
563 *PHENIX* [78].
564 The structures were validated using *Coot*, MolProbity [79] and wwPDB Validation Service
565 (https://validate.wwpdb.org) [80]. Statistics for data collection, refinement, and model quality are
566 listed in Supplementary Table 5. The structure factors and coordinates were deposited to the
567 Protein Data Bank with accession codes 5U9Z (apo eGacH) and 6DGM (GroP•eGacH
568 complex). Structure figures were generated using PyMOL v1.8.0.3 [81].
569 **Isolation of cell wall**
570 Cell wall was isolated from exponential phase cultures by the SDS-boiling procedure as
571 described for *S. pneumoniae* [82]. Purified cell wall samples were lyophilized and used for
572 carbohydrate composition analysis, phosphate and glycerol assays. Cell wall isolated from GAS
573 5005 was used for purification of GAC for *sn*-glycerol-1-phosphate identification and NMR
574 analysis.
575 **GAC purification**
576 GAC was released from the cell wall by sequential digestion with mutanolysin (Sigma Aldrich)
577 and recombinant PlyC amidase [19], and partially purified by a combination of SEC and ion-
578 exchange chromatography. Mutanolysin digests contained 5 mg/mL of cell wall suspension in
579 0.1 M sodium acetate, pH 5.5, 2 mM $CaCl_2$ and 5 U/mL mutanolysin. Following overnight
580 incubation at 37 °C, soluble polysaccharide was separated from the cell wall by centrifugation at
581 13,000 x g, 10 min. Acetone (-20 °C) was added to a final concentration of 80% and the
582 polysaccharide was allowed to precipitate overnight at -20 °C. The precipitate was sedimented
583 (5,000 x g, 20 min), dried briefly under nitrogen gas and redissolved in 0.1 M Tris-Cl, pH 7.4
584 PlyC (50 μg/mL) was added to the GAC sample and the reaction was incubated overnight at
585 37 °C. Following PlyC digestion, GAC was recovered by acetone precipitation, as described
586 above, redissolved in a small volume of 0.2 N acetic acid and chromatographed on a 25 mL
587 column of BioGel P10 equilibrated in 0.2 N acetic acid. Fractions (1.5 mL) were collected and
588 monitored for carbohydrate by the anthrone assay. Fractions containing GAC (eluting near the
589 void volume of the column) were combined, concentrated by spin column centrifugation (3,000
590 MW cutoff filter) and desalted by several rounds of dilution with water and centrifugation. After
591 desalting, GAC was loaded onto an 18 mL column of DEAE-Sephacel. The column was eluted
592 with a 100 mL gradient of NaCl (0-1 M). Fractions were analyzed for carbohydrate by the
593 anthrone assay and phosphate by the malachite green assay following digestion with 70%
594 perchloric acid (see below). Fractions containing peaks of carbohydrate were combined,
595 concentrated by spin column (3,000 MW cut off) and lyophilized.

596 **Anthrone assay**

597 Total carbohydrate content was determined by a minor modification of the anthrone procedure.
598 Reactions containing 0.08 mL of aqueous sample and water were prepared in Safe-Lock 1.5 mL
599 Eppendorf Tubes. Anthrone reagent (0.2% anthrone, by weight, dissolved in concentrated
600 H_2SO_4) was rapidly added, mixed thoroughly, capped tightly and heated to 100 °C, 10 min. The
601 samples were cooled in water (room temperature) and the absorbance at 580 nm was recorded.
602 GAC concentration was estimated using an L-Rha standard curve.

603 **Phosphate assay**

604 Approximately 1.5 mg of cell wall material isolated from GAS was dissolved in 400 μL H_2O and
605 8 μg/mL PlyC, and incubated at 37 °C, rotating for approximately 16 hrs. Additional PlyC was
606 added and incubated for a further 4-6 hrs. To liberate SCC from *S. mutans* cell wall, 1.5 mg of
607 cell wall material isolated from *S. mutans* were incubated 24 h with 1.5 U/mL mutanolysin in
608 400 μL of 0.1 M sodium acetate, pH 5.5, 2 mM $CaCl_2$. The samples were incubated at 100 °C
609 for 20 min and centrifuged for 5 min at maximum speed in a table top centrifuge. The
610 supernatant was transferred to a new micro-centrifuge tube and incubated with 2 N HCl at
611 100 °C for 2 hrs. The samples were neutralized with NaOH, in the presence of 62.5 mM
612 HEPES pH 7.5. To 100 μL of acid hydrolyzed sample, 2 μL of 1 U/μL alkaline phosphatase
613 (Thermo Fisher) and 10 μL 10 x alkaline phosphatase buffer was added and incubated at 37 °C,
614 rotating, overnight. Released phosphate was measured using the Pi ColorLock Gold kit (Innova
615 Biosciences), according to the manufacturer's protocol.

616 During GAC purification on BioGel P10 and DEAE-Sephacel total phosphate content
617 was determined by the malachite green method following digestion with perchloric acid.
618 Fractions containing 10 to 80 μL were heated to 110 °C with 40 μL 70% perchloric acid (Fisher
619 Scientific) in 13 x 100 borosilicate disposable culture tubes for 1 h. The reactions were diluted to
620 160 μL with water and 100 μL was transferred to a flat-bottom 96-well culture plate. Malachite
621 Green reagent (0.2 mL) was added and the absorbance at 620 nm was read after 10 min at
622 room temperature. Malachite Green reagent contained 1 vol 4.2% ammonium molybdate
623 tetrahydrate (by weight) in 4 M HCl, 3 vol 0.045% malachite green (by weight) in water and
624 0.01% Tween 20.

625 **Glycerol assay**

626 Samples for glycerol measurement were prepared as described for the phosphate assay but
627 were not digested with alkaline phosphatase. Instead glycerol concentration was measured
628 using the Glycerol Colorimetric assay kit (Cayman Chemical) according to the manufacturer's
629 protocol.

630 **Carbohydrate composition analysis**

631 Carbohydrate composition analysis was performed at the Complex Carbohydrate Research
632 Center (Athens, GA) by combined gas chromatography/mass spectrometry (GC/MS) of the per-
633 O-trimethylsilyl derivatives of the monosaccharide methyl glycosides produced from the sample
634 by acidic methanolysis as described previously [83].

635 **Identification of the stereochemistry of the GroP moiety of GAC**

636 The stereochemistry of the GroP moiety attached to GAC was determined by a chemo-
637 enzymatic method following release of GroP by alkaline hydrolysis as described by Kennedy *et*
638 *al.* [32] using the Amplite™ Fluorimetric *sn*-Glycerol-3-Phosphate (Gro-3-P) Assay Kit (AAT
639 Bioquest). GAC was released from cell wall by sequential digestion with mutanolysin hydrolase
640 and PlyC amidase, and partially purified by SEC on BioGel P10 and ion exchange
641 chromatography on DEAE-Sephacel, as described above. GroP was liberated from the GAC by
642 alkaline hydrolysis (0.5 M NaOH, 100 °C, 1 h), neutralized with acetic acid and recovered from
643 the inclusion volume following SEC on BioGel P10. Column fractions containing GroP were
644 identified by HPLC/mass spectrometry (LC-MS) and fractions containing GroP were combined,
645 concentrated by rotary evaporation (30 °C, under reduced pressure) and desalted on BioGel P2.
646 Column fractions containing GroP were combined, lyophilized and analyzed with the Gro-3-P
647 Assay Kit based on the production of hydrogen peroxide in the *sn*-Gro-3-P oxidase-mediated
648 enzyme coupled reaction. Reactions were conducted at room temperature for 10 to 20 min in
649 solid black 96 well plates in a total volume of 0.1 ml. Excitation was at 540 nm and fluorescence
650 at 590 nm was measured.

651 The fractions containing GroP were analyzed by LC-MS using a Q Exactive mass
652 spectrometer and an Ultimate 3000 ultra high performance liquid chromatography system
653 (Thermo Fisher Scientific). Chromatographic separation was achieved using a silica-based
654 SeQuant ZIC-pHILIC column (2.1 mm × 150 mm, 5 μm, Merck, Germany) with elution buffers
655 consisting of (A) 20 mM $(NH_4)_2CO_3$ with 0.1% NH_4OH in H_2O and (B) acetonitrile. The column
656 temperature was maintained at 40 °C, and the flow rate was set to 150 μL/min. Mass
657 spectrometric detection was performed by electrospray ionization in negative ionization mode
658 with source voltage maintained at 3.0 kV. The capillary temperature, sheath gas flow and
659 auxiliary gas flow were set at 275 °C, 40 arb and 15 arb units, respectively. Full-scan MS
660 spectra (mass range m/z 75 to 1000) were acquired with resolution R = 70,000 and AGC target
661 1e6.

662 **Identification of hGIIA-resistant GAS transposon mutants**

663 The GAS M1T1 5448 *Krmit* transposon mutant library [14] was grown to mid-log phase (OD_{600} =
664 0.4). 1 x 10^5 CFU were subjected to 27.5 μg/mL recombinant hGIIA [84] in triplicate and incubated
665 for 1 h at 37 °C. Samples were plated on THY agar plates supplemented with kanamycin. The
666 position of the transposon insertion of resistant colonies was determined as described
667 previously [85].

668 **hGIIA susceptibility assay**

669 hGIIA susceptibility experiments were performed as described previously [21]. In short, mid-log
670 suspensions (OD_{600} = 0.4), of GAS and *S. mutans* were diluted 1,000 times in HEPES solution
671 (20 mM HEPES, 2 mM Ca^{2+}, 1% BSA [pH 7.4]) and 10 μL was added to sterile round-bottom 96
672 well plates in triplicates. Recombinant hGIIA was serially diluted in HEPES solution and 10 μL
673 aliquots were added to bacteria-containing wells. Samples were incubated for 2 hrs at 37 °C (for
674 GAS without CO_2, for *S. mutans* with 5% CO_2), PBS was added and samples were 10-fold
675 serially diluted for quantification on agar plates. Survival rate was calculated as Survival (% of
676 inoculum) = (counted CFU * 100) / CFU count of original.

677 **Determination of selective metal concentrations**

678 The Zn^{2+} sensitive gene deletion mutant 5448Δ*czcD* [24] was used to find the target concentration
679 of Zn^{2+}. Briefly, colonies of strains 5448 WT and 5448Δ*czcD* were scraped from THY agar
680 plates and resuspended in PBS. After washing in PBS, the strains were adjusted to OD_{600} =1.
681 These cultures were used to inoculate freshly prepared mRPMI containing varying
682 concentrations of Zn^{2+} to starting OD_{600} = 0.05 in a 96-well plate. Growth at 37 °C was
683 monitored at OD_{595} every 15 min using the BMG Fluostar plate reader.

684 **Tn-seq library screen for Zn^{2+} sensitivity**

685 The 5448 *Krmit* Tn-seq library at T_0 generation [14] was thawed, inoculated into 150 mL
686 prewarmed THY broth containing 300 μg/mL kanamycin and grown at 37 °C for 6 hrs. After 6
687 hrs growth, the culture (T_1) was centrifuged at 4,000 x *g* for 15 min at 4 °C and the pellet
688 resuspended in 32.5 mL saline. Freshly prepared mRPMI or mRPMI containing 10 μM or 20 μM
689 Zn^{2+} was inoculated with 500 μL culture into 39.5 mL media, creating a 1:20 fold inoculation.
690 These T_2 cultures were then grown at 37 °C for exactly 6 hrs, at which point 2 mL of these
691 cultures were inoculated again into 38 mL of freshly prepared mRPMI alone or mRPMI
692 containing 10 μM or 20 μM Zn^{2+}. The remaining 38 mL of T_2 culture was harvested by
693 centrifugation at 4,000 x *g* for 10 min at 4 °C and pellets stored at -20 °C for later DNA
694 extraction. Cultures were grown for a further 6 hrs, at which point T_3 cultures were harvested by
695 centrifugation at 4,000 x *g* for 10 min at 4 °C and pellets stored at -20 °C.

696 Tn-seq *Krmit* transposon insertion tags were prepared from the cell pellets as previously
697 described [15,86]. Briefly, genomic DNA was prepared using the MasterPure complete DNA and
698 RNA purification kit (Epicentre) and treated with *MmeI* and the calf intestinal phosphatase (NEB)
699 before ligation to 12 distinct Tn-seq adapters for sample multiplexing during massively parallel
700 sequencing [15,86]. Insertion tags were produced through a 22-cycle PCR [15] using the ligation
701 mixtures and primers oKrmitTNseq2 and AdapterPCR [15,86]. After quality control with the
702 Bioanalyzer instrument (Agilent), the libraries of *Krmit* insertion tags were sequenced (50-nt
703 single end reads) on an Illumina HiSeq 1500 in the Institute for Bioscience and Biotechnology
704 Research (IBBR) Sequencing Core at the University of Maryland, College Park. Tn-seq read
705 datasets were analyzed (quality, filtering, trimming, alignment, visualization) as previously
706 described [15,86] using the M1T1 5448 genome as reference for read alignments. The ratios of
707 mutant abundance comparing the output to input mutant pools were calculated as a fold change
708 for each GAS gene using the DEseq2 and EdgeR pipelines [86-88]. Illumina sequencing reads from
709 the Tn-seq analysis were deposited in the NCBI Sequence Read Archive (SRA) under the
710 accession number SRP150081.

711 **Drop test assays**

712 Strains 5448 WT, 5448Δ*gacI*, 5448Δ*gacI:gacI*, 5448Δ*gacH*, 5448Δ*gacH*:p*gacH*, *S. mutans* WT,
713 SMUΔ*sccH*, SMUΔ*sccH:*p*sccH* and SMUΔ*sccH:*p*gacH* were grown in THY to mid-exponential
714 growth phase, adjusted to OD_{600} = 0.6 and serial diluted. 5 μL were spotted onto THY agar
715 plates containing varying concentrations of Zn^{2+} ($ZnSO_4 \cdot 7H_2O$). Plates were incubated at 37 °C
716 overnight and photographed. Drop tests are representative of biological replicates performed on
717 at least 3 separate occasions.

718 **NMR spectroscopy**

719 The NMR spectra were recorded on a Bruker AVANCE III 700 MHz equipped with a 5 mm TCI
720 Z-Gradient Cryoprobe ($^1H/^{13}C/^{15}N$) and dual receivers and a Bruker AVANCE II 600 MHz
721 spectrometer equipped with a 5 mm TXI inverse Z-Gradient $^1H/D-^{31}P/^{13}C$. The ^1H and ^{13}C NMR
722 chemical shift assignments of the polysaccharide material were carried out in D_2O solution
723 (99.96 %) at 323.2 K unless otherwise stated. Chemical shifts are reported in ppm using internal
724 sodium 3-trimethylsilyl-(2,2,3,3-$^2H_4$)-propanoate (TSP, δ_H 0.00 ppm), external 1,4-dioxane in
725 D_2O (δ_C 67.40 ppm) and 2 % H_3PO_4 in D_2O (δ_P 0.00 ppm) as reference. The $^1H,^1H$-TOCSY
726 experiments (dipsi2ph) were recorded with mixing times of 10, 30, 60, 90 and 120 ms. The
727 $^1H,^1H$-NOESY experiments [89] were collected with mixing times of 100 and 200 ms. A uniform
728 and non-uniform sampling (50 and 25 % NUS) were used for the multiplicity-edited $^1H,^{13}C$-
729 HSQC experiments [90] employing an echo/antiecho-TPPI gradient selection with and without

730 decoupling during the acquisition. The 2D $^{1}H,^{13}C$-HSQC-TOCSY were acquired using MLEV17
731 for homonuclear Hartman-Hahn mixing, an echo/antiecho-TPPI gradient selection with
732 decoupling during acquisition and mixing times of 20, 40, 80 and 120 ms. The 2D $^{1}H,^{31}P$-Hetero-
733 TOCSY experiments [91] were collected using a DIPSI2 sequence with mixing times of 10, 20, 30,
734 50 and 80 ms. The 2D $^{1}H,^{31}P$-HMBC experiments were recorded using an echo/antiecho
735 gradient selection and mixing times of 25, 50 and 90 ms. The 3D $^{1}H,^{13}C,^{31}P$ [36] spectra were
736 obtained using echo/antiecho gradient selection and constant time in t_2 with a nominal value of
737 $^{n}J_{CP}$ of 5 Hz and without multiplicity selection. The spectra were processed and analyzed using
738 TopSpin 4.0.1 software (Bruker BioSpin).

739 **Bioinformatics analysis**

740 The TOPCONS (http://topcons.net/) [92] web server was employed to predict trans-membrane
741 regions of GacH. Homology detection and structure prediction were performed by the HHpred
742 server (https://toolkit.tuebingen.mpg.de/#/tools/hhpred) [93]. To construct the GacH phylogenetic
743 tree the homologues of full-length GacH (M5005_Spy_0609) were retrieved using blastp with an
744 E-value cutoff of $1e^{-70}$. In addition, sequences were filtered based on a minimal identity of 33%,
745 similarity of 73%, and having 11 predicted transmembrane helixes. Of all species expressing
746 *gacH* homologues, *ltaS* homologues were retrieved using blastp and GAS *ltaS*
747 (M5005_Spy_0622) as reference. As representatives of the LtaS and LtaP clades, five
748 sequences of Listeria were selected that express both enzymes [27]. All protein sequences were
749 aligned using MUSCLE [94]. The phylogenetic tree was build using MEGA6 [95] and the Maximum
750 Likelihood method based on the JTT matrix-based model [95]. For the phylogenetic tree with the
751 extracellular domains of GacH and LtaS homologues, extracellular domains were predicted
752 using http://www.cbs.dtu.dk/services/TMHMM/.

753 **Statistical analysis**

754 Unless otherwise indicated, statistical analysis was carried out on pooled data from at least
755 three independent biological repeats. Quantitative data was analyzed using the paired Student's
756 t-test. A 2-way ANOVA with Bonferroni multiple comparison test was used to compare multiple
757 groups. A *P*-value equal to or less that 0.05 was considered statistically significant.

758

759 **Acknowledgements**

760 This work was supported by the Center of Biomedical Research Excellence (COBRE) Pilot
761 Grant (to NK, KVK and JSR) supported by NIH grant P30GM110787 from the National Institute
762 of General Medical Sciences (NIGMS), VIDI grant 91713303 from the Netherlands Organization
763 for Scientific Research (NWO) (to NMvS and VPvH), the Swedish Research Council (no. 2013-

764 4859 and 2017-03703) and The Knut and Alice Wallenberg Foundation (to GW), NIH grant
765 P30GM110787 from the NIGMS and NIH grant 1S10OD021753 (to AJM), the National Health
766 and Medical Research Council of Australia (to MJW), grants from CNRS, ANR (MNaims ANR-
767 17-CE17-0012-01) and FRM (SPF20150934219) (to GL), NIH grant AI047928 from the National
768 Institute of Allergy and Infectious Diseases (NIAID) (to KSM and YLB) and NIH grant AI094773
769 (to NES and ATB).
770 Carbohydrate composition analysis at the Complex Carbohydrate Research Center was
771 supported by the Chemical Sciences, Geosciences and Biosciences Division, Office of Basic
772 Energy Sciences, U.S. Department of Energy grant (DE-FG02-93ER20097) to Parastoo Azadi.
773 Use of the Advanced Photon Source was supported by the U. S. Department of Energy, Office
774 of Science, Office of Basic Energy Sciences, under Contract No. W-31-109-Eng-38 and NIH
775 grants S10_RR25528 and S10_RR028976. Use of the Stanford Synchrotron Radiation
776 Lightsource, SLAC National Accelerator Laboratory, is supported by the U.S. Department of
777 Energy, Office of Science, Office of Basic Energy Sciences under Contract No. DE-AC02-
778 76SF00515. The SSRL Structural Molecular Biology Program is supported by the DOE Office of
779 Biological and Environmental Research, and by the NIH, NIGMS including P41GM103393. The
780 contents of this publication are solely the responsibility of the authors and do not necessarily
781 represent the official views of NIGMS or NIH.
782
783
784 **Author contributions**
785 AR, PD, YLB, KSM, AGM, AJM, GL, MJW, JSR, KVK, GW, NMvS and NK designed the
786 experiments. RJE, VPvH, AR, AT, JSR, KVK, GW and NK performed functional and
787 biochemical experiments. KVK carried out X-ray crystallography and structure analysis. AR and
788 GW performed NMR studies. PD and AJM performed MS analysis. VPvH and NK constructed
789 plasmids and isolated mutants. RJE, VPvH, AR, PD, YLB, NMES, ATB, KSM, AGM, AJM, MJW,
790 JSR, KVK, GW, NMvS and NK analyzed the data. NMvS and NK wrote the manuscript with
791 contributions from all authors. All authors reviewed the results and approved the final version of
792 the manuscript.
793

794 **Figures**

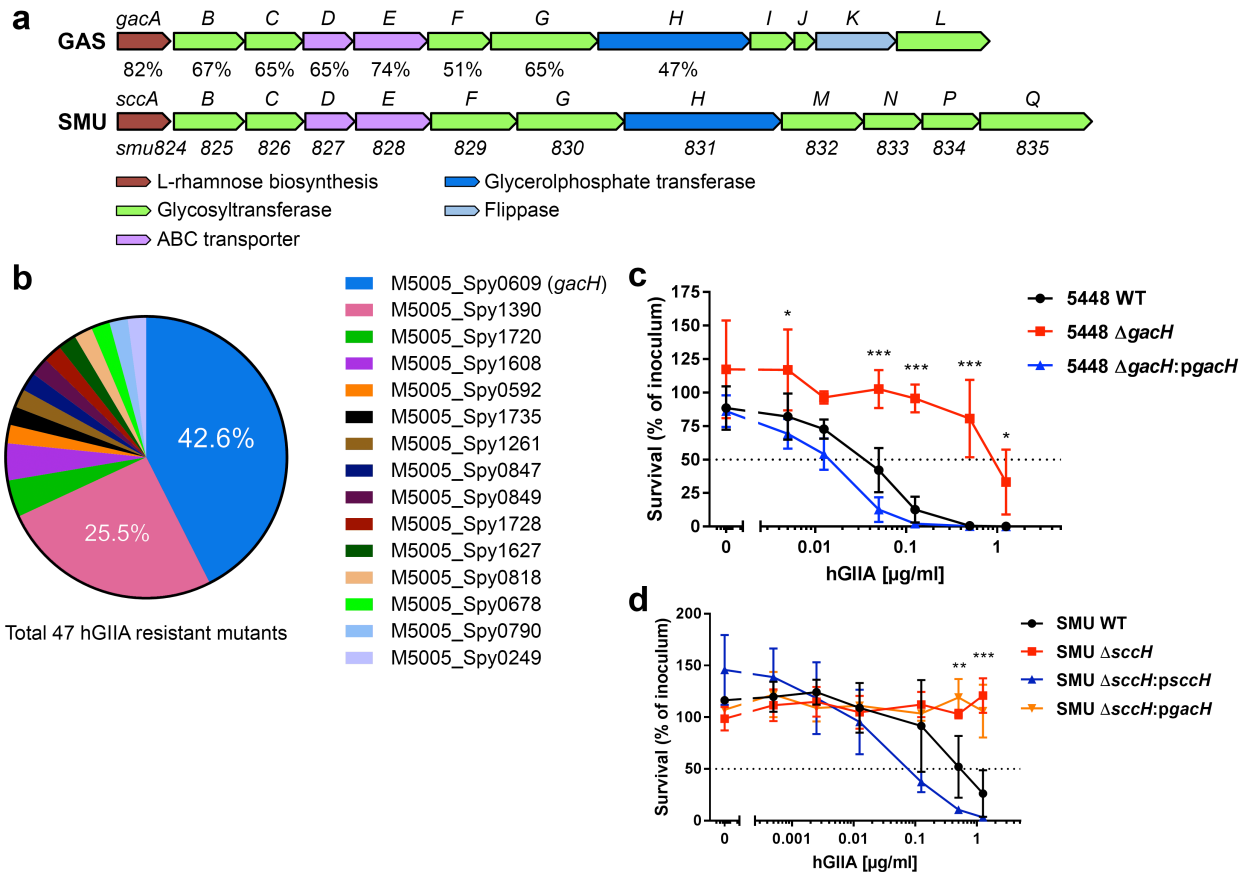

795

796 **Fig. 1. GacH homologues are required for full hGIIA bactericidal activity against GAS and**
797 ***S. mutans.***
798 (**a**) Schematic representation of GAC and SCC biosynthetic gene clusters. SCC gene cluster
799 *smu*824-835 was renamed *sccABCDEFGHMNPQ*. Sequence identity (%) between homologous
800 proteins is indicated. Sequences of GAS 5005 and *S. mutans* UA159 were used for comparison.
801 (**b**–**d**) *gacH* is identified in Tn-seq screen for hGIIA resistance and its deletion confers
802 resistance to hGIIA**.** (**b**) Transposon gene location in 47 hGIIA resistant mutants after exposure
803 of *Krmit* mutant transposon library to lethal concentrations of hGIIA. (**c**) Deletion of *gacH* in
804 GAS 5448 and (**d**) the *gacH*-homologous gene *sccH* in *S. mutans* increases hGIIA resistance
805 more than 10-fold. Data represent mean ± standard deviation of three independent experiments.
806 *, $p < 0.05$; **, $p < 0.01$; ***, $p < 0.001$.

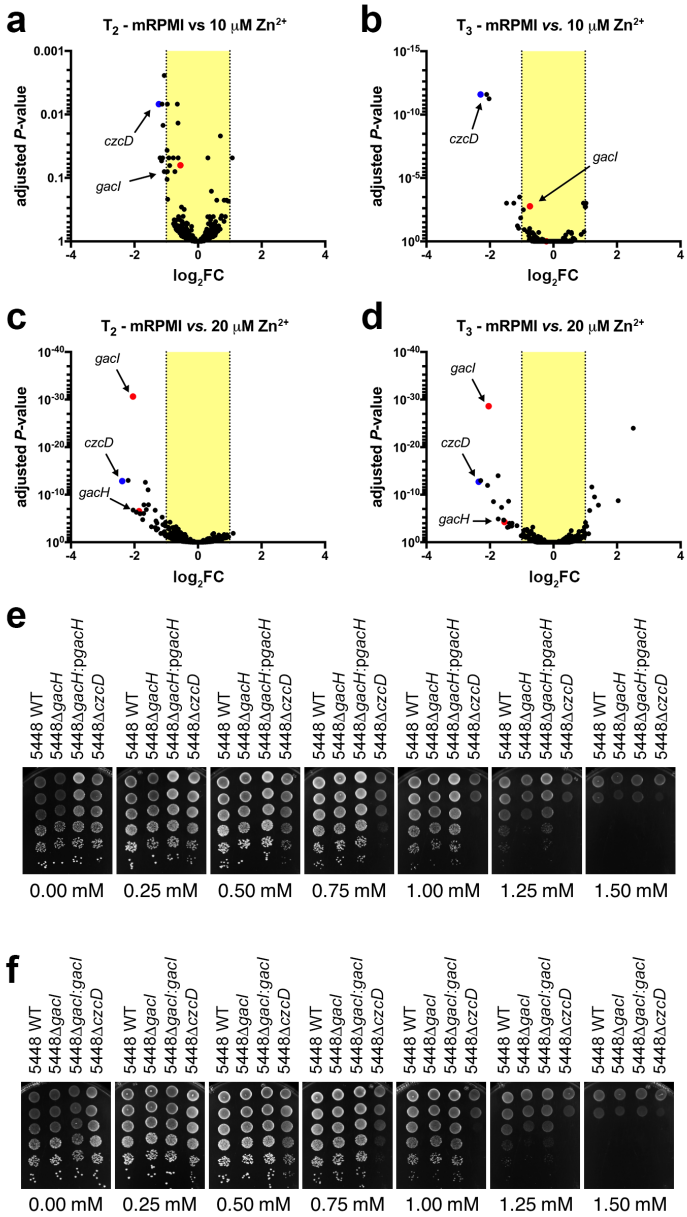

Fig. 2. Deletion of *gacI* and *gacH* renders GAS susceptible to Zn^{2+}.
(**a**–**d**) Tn-seq volcano plots showing representation of *czcD*, *gacH* and *gacI* in GAS *Krmit* transposon library screens for Zn^{2+} tolerance. Log_2 fold-change (log_2 FC) in fitness was plotted against adjusted *P*-value from Tn-seq analysis. The outline of the experiment is shown in Supplemental Fig. 2b. Tn-seq screens of the transposon library were conducted using (**a**) 10 μM Zn^{2+} at T_2, (**b**) 10 μM Zn^{2+} at T_3, (**c**) 20 μM Zn^{2+} at T_2, (**d**) 20 μM Zn^{2+} at T_3.
(**e** and **f**) Zn^{2+} sensitivity as tested in drop test assay using strains (**e**) 5448 WT, 5448Δ*gacH* and 5448Δ*gacH*:p*gacH*; and (**f**) 5448 WT, 5448Δ*gacI* and 5448Δ*gacI:gacI*. 5448Δ*czcD* was included as a positive control in both panels. Strains were grown in THY to mid-exponential phase, adjusted to OD_{600} = 0.6, serial diluted and 5 μL spotted onto THY agar plates containing varying concentrations of Zn^{2+}. Each drop test assay experiment was performed at least three times.

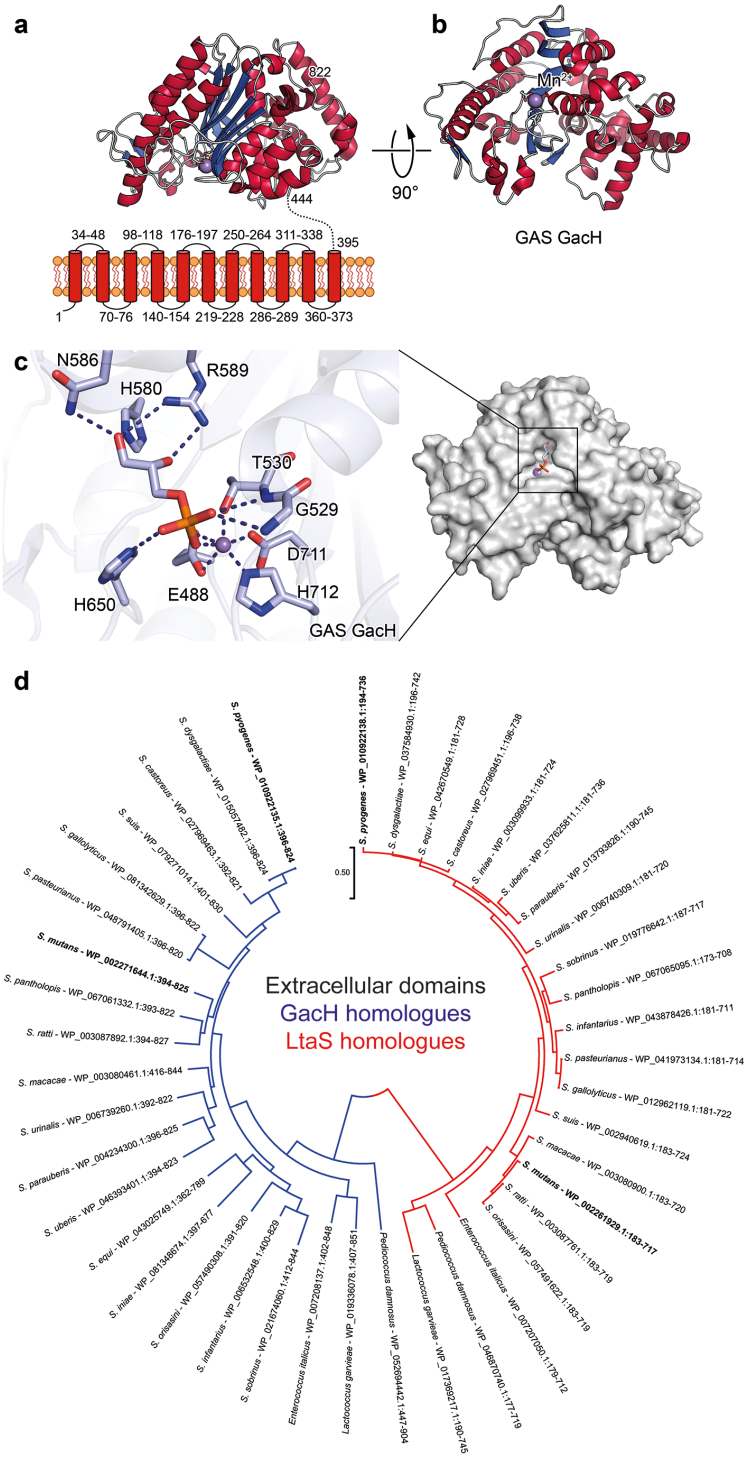

Fig. 3. Structure of GacH and phylogenetic analysis of the GacH family of proteins. (**a**) Predicted topology of GacH showing eleven transmembrane helices and structure of extracellular domain with the enzymatic active site oriented towards the cell membrane. (**b**) Structure of apo eGacH viewing at the active site with the Mn^{2+} ion shown as a violet sphere. (**c**) A close-up view of the active site GacH crystal structure in complex with *sn*-Gro-1-P. (**d**) Phylogenetic analysis by Maximum Likelihood method of the predicted extracellular domains of

826 GacH and LtaS enzymes. A phylogenetic tree was generated using the predicted extracellular
827 domains of 21 GacH (blue) and 21 LtaS (red) homologues from the same species. The GAS
828 and *S. mutans* proteins analyzed in this study are indicated in bold. The phylogenetic tree is
829 drawn to scale as indicated by the scale bar, with branch lengths measured in the number of
830 substitutions per site.
831

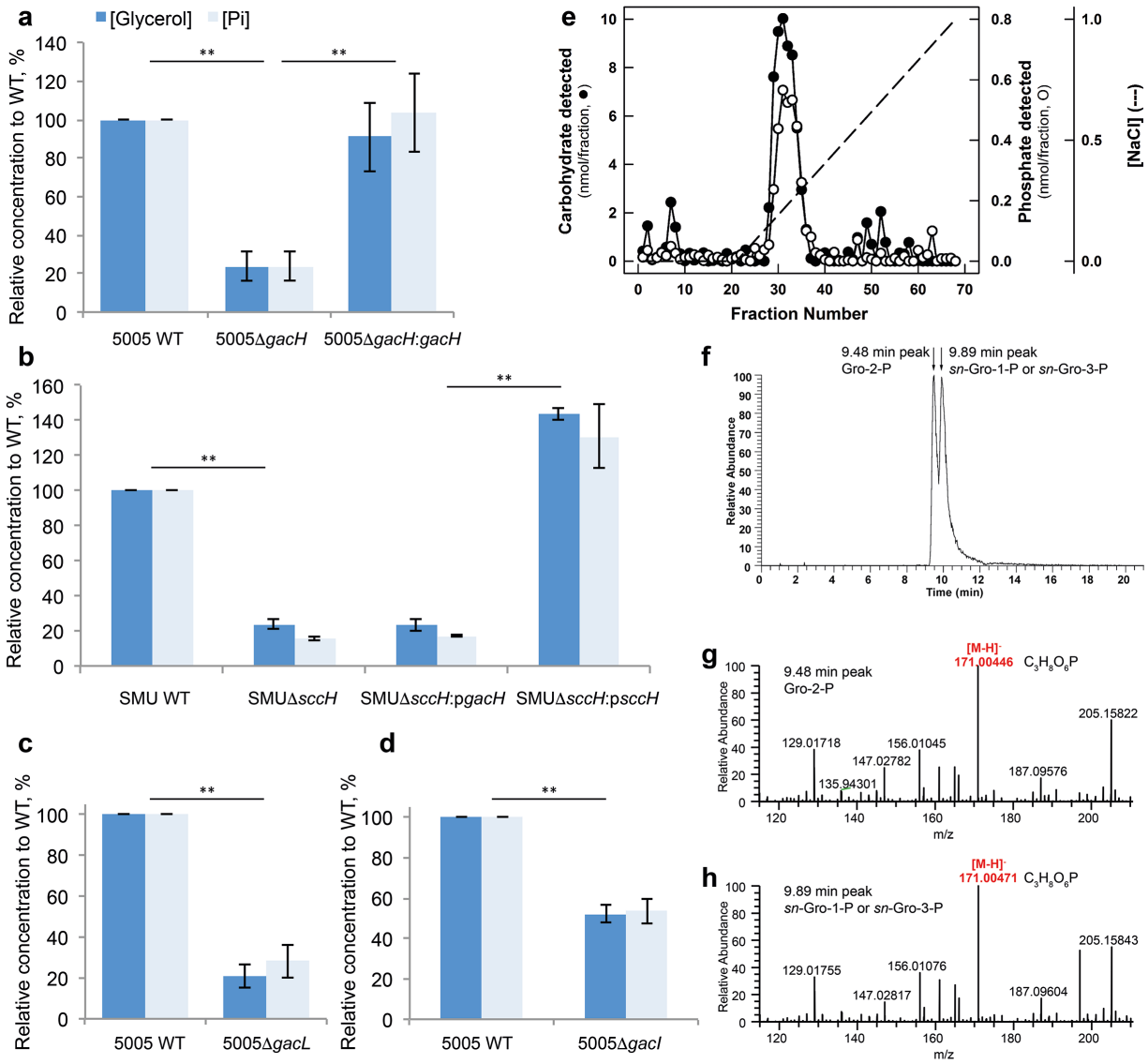

Fig. 4. GacH and SccH modify SRPs with *sn*-Gro-1-P.
(**a**-**d**) Analysis of glycerol and phosphate content in GAC and SCC isolated from (**a**) GAS 5005 WT, Δ*gacH* and complemented strain; (**b**) *S. mutans* WT, Δ*sccH*, and Δ*sccH* complemented with *sccH* or *gacH*, and (**c** and **d**) GAS 5005 mutants Δ*gacL* and Δ*gacI* that are devoid of GlcNAc side-chain. GAC and SCC were released from bacterial cell wall materials by PlyC and mutanolysin digestion, respectively, and subjected to acid hydrolysis as described in Methods. Phosphate was released from these samples by digestion with alkaline phosphatase and measured using the malachite green assay. Glycerol was measured using a colorimetric glycerol assay kit. The concentration of phosphate and glycerol is presented relative to the WT strain. Data are mean ± standard deviation of three independent replicates. **, $p < 0.01$. *P*-values are shown for glycerol and phosphate concentrations. (**e**) DEAE-Sephacel elution profile of GAC. Isolated GAC was loaded onto an 18 mL column of DEAE-Sephacel. The column was eluted with a 100 ml gradient of NaCl (0-1 M). Fractions were analyzed for carbohydrate by anthrone assay (●) and phosphate by malachite green assay (O). (**f**–**h**) Identification of the

847 enantiomeric form of GroP associated with GAC. (**f**) The GroP isomers were recovered from
848 GAC following alkaline hydrolysis and separated by liquid chromatography as outlined in
849 Methods. The elution positions corresponding to standard Gro-2-P and *sn*-Gro-1-P/*sn*-Gro-3-P
850 are indicated by the arrows. LC-MS analysis identifies two extracted ion chromatogram peaks
851 for the molecular GroP ion *m/z* 171.004 $[M-H]^-$, which eluted at (**g**) 9.48 and (**h**) 9.89 min. Based
852 on the accurate mass and retention times, these two peaks were assigned as Gro-2-P and *sn*-
853 Gro-1-P/*sn*-Gro-3-P respectively by comparison with authentic chemical standards.

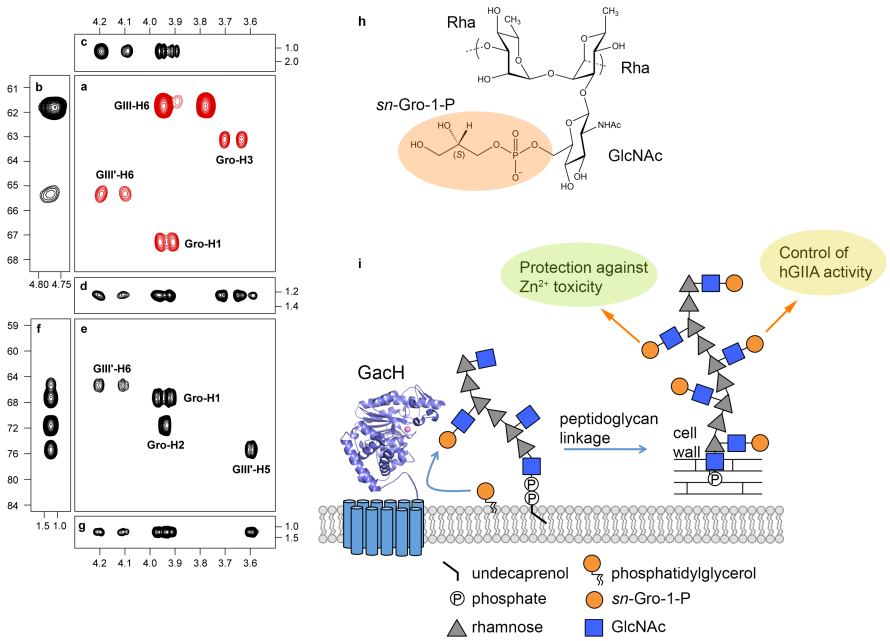

854

855 **Fig. 5. NMR analysis confirms presence of GroP on GlcNAc hydroxymethyl group of**
856 **GAC.**
857 (**a**-**g**) Selected regions of NMR spectra of GAC. (**a**) Multiplicity-edited ^{1}H,^{13}C-HSQC in which
858 methylene groups have opposite phase and are shown in red color, (**b**) ^{1}H,^{13}C-HSQC-TOCSY
859 with an isotropic mixing time of 120 ms, (**c**) ^{1}H,^{13}C-HMBC with a mixing time of 90 ms, (**d**)
860 ^{1}H,^{31}P-hetero-TOCSY with an isotropic mixing time of 80 ms, (**e**) ^{1}H,^{13}C-plane, (**f**) ^{13}C, ^{31}P-plane
861 using a nominal $^{n}J_{CP}$ value of 5 Hz, and (**g**) ^{1}H, ^{31}P-plane of a through-bond 3D ^{1}H,^{13}C,^{13}P NMR
862 experiment. Cross-peaks are annotated as GIII corresponding to the GlcNAc residue, GIII' being
863 the GroP-substituted GlcNAc residue and Gro as the glycerol residue. NMR chemical shifts of
864 ^{1}H (horizontal axis), ^{13}C (left axis) and ^{31}P (right axis and panel **f**) are given in ppm.
865 (**h**) Schematic structure of the GAC repeating unit consisting of →3)-α-L-Rha*p*-(1→2)[β-D-
866 Glc*p*NAc6*P*(*S*)Gro-(1→3)]-α-L-Rha*p*-(1→. (**i**) The mechanism and the roles of GroP cell wall
867 modification in streptococci.

868 **References**

869

870 1. Brown, S., Santa Maria, J.P., Jr. & Walker, S. Wall teichoic acids of Gram-positive
871 bacteria. *Annu. Rev. Microbiol.* **67**, 313-336 (2013).
872 2. Neuhaus, F.C. & Baddiley, J. A continuum of anionic charge: structures and functions of
873 D-alanyl-teichoic acids in Gram-positive bacteria. *Microbiol. Mol. Biol. Rev.* **67**, 686-723
874 (2003).
875 3. Weidenmaier, C. & Peschel, A. Teichoic acids and related cell-wall glycopolymers in
876 Gram-positive physiology and host interactions. *Nat. Rev. Microbiol.* **6**, 276-287 (2008).
877 4. Mistou, M.Y., Sutcliffe, I.C. & van Sorge, N.M. Bacterial glycobiology: rhamnose-
878 containing cell wall polysaccharides in Gram-positive bacteria. *FEMS Microbiol. Rev.* **40**,
879 464-479 (2016).
880 5. McCarty, M. The lysis of group A hemolytic streptococci by extracellular enzymes of
881 *Streptomyces albus*. II. Nature of the cellular substrate attacked by the lytic enzymes. *J.*
882 *Exp. Med.* **96**, 569-580 (1952).
883 6. Lancefield, R.C. A serological differentiation of human and other groups of hemolytic
884 Streptococci. *J. Exp. Med.* **57**, 571-595 (1933).
885 7. Huang, D.H., Rama Krishna, N. & Pritchard, D.G. Characterization of the group A
886 streptococcal polysaccharide by two-dimensional ^{1}H-nuclear-magnetic-resonance
887 spectroscopy. *Carbohydr. Res.* **155**, 193-199 (1986).
888 8. St Michael, F. et al. Investigating the candidacy of the serotype specific rhamnan
889 polysaccharide based glycoconjugates to prevent disease caused by the dental
890 pathogen *Streptococcus mutans*. *Glycoconj. J.* **35**, 53-64 (2018).
891 9. van der Beek, S.L. et al. GacA is essential for Group A Streptococcus and defines a new
892 class of monomeric dTDP-4-dehydrorhamnose reductases (RmlD). *Mol. Microbiol.* **98**,
893 946-962 (2015).
894 10. Tsuda, H., Yamashita, Y., Shibata, Y., Nakano, Y. & Koga, T. Genes involved in
895 bacitracin resistance in *Streptococcus mutans*. *Antimicrob. Agents Chemother.* **46**,
896 3756-3764 (2002).
897 11. De, A. et al. Deficiency of RgpG causes major defects in cell division and biofilm
898 formation, and deficiency of LytR-CpsA-Psr family proteins leads to accumulation of cell
899 wall antigens in culture medium by *Streptococcus mutans*. *Appl. Environ. Microbiol.* **83**,
900 e00928 (2017).
901 12. Nagata, E. et al. Serotype-specific polysaccharide of *Streptococcus mutans* contributes
902 to infectivity in endocarditis. *Oral. Microbiol. Immunol.* **21**, 420-423 (2006).
903 13. van Sorge, N.M. et al. The classical Lancefield antigen of Group A Streptococcus is a
904 virulence determinant with implications for vaccine design. *Cell Host Microbe* **15**, 729-
905 740 (2014).
906 14. Le Breton, Y. et al. Essential genes in the core genome of the human pathogen
907 *Streptococcus pyogenes*. *Sci. Rep.* **5**, 9838 (2015).
908 15. Henningham, A. et al. Virulence role of the GlcNAc side chain of the Lancefield cell wall
909 carbohydrate antigen in non-M1-serotype Group A Streptococcus. *mBio* **9**, e02294
910 (2018).
911 16. Kabanova, A. et al. Evaluation of a Group A Streptococcus synthetic oligosaccharide as
912 vaccine candidate. *Vaccine* **29**, 104-114 (2010).
913 17. Sabharwal, H. et al. Group A streptococcus (GAS) carbohydrate as an immunogen for
914 protection against GAS infection. *J. Infect. Dis.* **193**, 129-135 (2006).
915 18. Shibata, Y., Yamashita, Y., Ozaki, K., Nakano, Y. & Koga, T. Expression and
916 characterization of streptococcal *rgp* genes required for rhamnan synthesis in
917 *Escherichia coli*. *Infect. Immun.* **70**, 2891-2898 (2002).

19. Rush, J.S. et al. The molecular mechanism of N-acetylglucosamine side-chain attachment to the Lancefield group A carbohydrate in *Streptococcus pyogenes*. *J. Biol. Chem.* **292**, 19441-19457 (2017).
20. Ozaki, K. et al. A novel mechanism for glucose side-chain formation in rhamnose-glucose polysaccharide synthesis. *FEBS Lett.* **532**, 159-163 (2002).
21. van Hensbergen, V.P. et al. Streptococcal Lancefield polysaccharides are critical cell wall determinants for human Group IIA secreted phospholipase A2 to exert its bactericidal effects. *PLoS Pathog.* **14**, e1007348 (2018).
22. Weiss, J.P. Molecular determinants of bacterial sensitivity and resistance to mammalian Group IIA phospholipase A2. *Biochim. Biophys. Acta.* **1848**, 3072-3077 (2015).
23. Graham, M.R. et al. Virulence control in group A Streptococcus by a two-component gene regulatory system: global expression profiling and *in vivo* infection modeling. *Proc. Natl. Acad. Sci. USA* **99**, 13855-13860 (2002).
24. Ong, C.L., Gillen, C.M., Barnett, T.C., Walker, M.J. & McEwan, A.G. An antimicrobial role for zinc in innate immune defense against group A streptococcus. *J. Infect. Dis.* **209**, 1500-1508 (2014).
25. Lu, D. et al. Structure-based mechanism of lipoteichoic acid synthesis by *Staphylococcus aureus* LtaS. *Proc. Natl. Acad. Sci. USA* **106**, 1584-1589 (2009).
26. Schirner, K., Marles-Wright, J., Lewis, R.J. & Errington, J. Distinct and essential morphogenic functions for wall- and lipo-teichoic acids in *Bacillus subtilis*. *EMBO J.* **28**, 830-842 (2009).
27. Campeotto, I. et al. Structural and mechanistic insight into the *Listeria monocytogenes* two-enzyme lipoteichoic acid synthesis system. *J. Biol. Chem.* **289**, 28054-28069 (2014).
28. Schneewind, O. & Missiakas, D. Lipoteichoic acids, phosphate-containing polymers in the envelope of Gram-positive bacteria. *J. Bacteriol.* **196**, 1133-1142 (2014).
29. Webb, A.J., Karatsa-Dodgson, M. & Grundling, A. Two-enzyme systems for glycolipid and polyglycerolphosphate lipoteichoic acid synthesis in *Listeria monocytogenes*. *Mol. Microbiol.* **74**, 299-314 (2009).
30. Emdur, L.I., Saralkar, C., McHugh, J.G. & Chiu, T.H. Glycerolphosphate-containing cell wall polysaccharides from *Streptococcus sanguis*. *J. Bacteriol.* **120**, 724-732 (1974).
31. Fischer, W., Laine, R.A. & Nakano, M. On the relationship between glycerophosphoglycolipids and lipoteichoic acids in Gram-positive bacteria. II. Structures of glycerophosphoglycolipids. *Biochim. Biophys. Acta* **528**, 298-308 (1978).
32. Kennedy, E.P., Rumley, M.K., Schulman, H. & Van Golde, L.M. Identification of *sn*-glycero-1-phosphate and phosphoethanolamine residues linked to the membrane-derived oligosaccharides of *Escherichia coli*. *J. Biol. Chem.* **251**, 4208-4213 (1976).
33. Orekhov, V.Y. & Jaravine, V.A. Analysis of non-uniformly sampled spectra with multi-dimensional decomposition. *Prog. Nucl. Magn. Reson. Spectrosc.* **59**, 271-292 (2011).
34. Widmalm, G. A perspective on the primary and three-dimensional structures of carbohydrates. *Carbohydr. Res.* **378**, 123-132 (2013).
35. Bernlind, C., Oscarson, S. & Widmalm, G. Synthesis, NMR, and conformational studies of methyl α-D-mannopyranoside 2-, 3-, 4-, and 6-monophosphates. *Carbohydr. Res.* **263**, 173-180 (1994).
36. Marino, J.P. et al. Three-dimensional triple-resonance ^{1}H, ^{13}C, ^{31}P experiment: sequential through-bond correlation of ribose protons and intervening phosphorus along the RNA oligonucleotide backbone. *J. Am. Chem. Soc.* **116**, 6472-6473 (1994).
37. Caliot, E. et al. Role of the Group B antigen of *Streptococcus agalactiae*: a peptidoglycan-anchored polysaccharide involved in cell wall biogenesis. *PLoS Pathog.* **8**, e1002756 (2012).
38. Coligan, J.E., Kindt, T.J. & Krause, R.M. Structure of the streptococcal groups A, A-variant and C carbohydrates. *Immunochemistry* **15**, 755-760 (1978).

969 39. Mc, C.M. & Lancefield, R.C. Variation in the group-specific carbohydrate of group A
970 streptococci. I. Immunochemical studies on the carbohydrates of variant strains. *J. Exp.*
971 *Med.* **102**, 11-28 (1955).
972 40. Pritchard, D.G., Coligan, J.E., Geckle, J.M. & Evanochko, W.T. High-resolution ^{1}H- and
973 ^{13}C-n.m.r. spectra of the group A-variant streptococcal polysaccharide. *Carbohydr. Res.*
974 **110**, 315-319 (1982).
975 41. Pritchard, D.G., Gregory, R.L., Michalek, S.M. & McGhee, J.R. Characterization of the
976 serotype e polysaccharide antigen of *Streptococcus mutans*. *Mol. Immunol.* **23**, 141-145
977 (1986).
978 42. Pritchard, D.G., Michalek, S.M., McGhee, J.R. & Furner, R.L. Structure of the serotype f
979 polysaccharide antigen of *Streptococcus mutans*. *Carbohydr. Res.* **166**, 123-131 (1987).
980 43. Heymann, H., Manniello, J.M. & Barkulis, S.S. Structure of streptococcal cell walls. V.
981 Phosphate esters in the walls of group A *Streptococcus pyogenes*. *Biochem. Biophys.*
982 *Res. Commun.* **26**, 486-491 (1967).
983 44. Pazur, J.H., Cepure, A., Kane, J.A. & Karakawa, W.W. Glycans from streptococcal cell
984 walls: glycosyl-phosphoryl moieties as immunodominant groups in heteroglycans from
985 group D and group L streptococci. *Biochem. Biophys. Res. Commun.* **43**, 1421-1428
986 (1971).
987 45. Prakobphol, A., Linzer, R. & Genco, R.J. Purification and characterization of a
988 rhamnose-containing cell wall antigen of *Streptococcus mutans* B13 (serotype d). *Infect.*
989 *Immun.* **27**, 150-157 (1980).
990 46. Czabanska, A., Holst, O. & Duda, K.A. Chemical structures of the secondary cell wall
991 polymers (SCWPs) isolated from bovine mastitis *Streptococcus uberis*. *Carbohydr. Res.*
992 **377**, 58-62 (2013).
993 47. Neiwert, O., Holst, O. & Duda, K.A. Structural investigation of rhamnose-rich
994 polysaccharides from *Streptococcus dysgalactiae* bovine mastitis isolate. *Carbohydr.*
995 *Res.* **389**, 192-195 (2014).
996 48. Karatsa-Dodgson, M., Wormann, M.E. & Grundling, A. *In vitro* analysis of the
997 *Staphylococcus aureus* lipoteichoic acid synthase enzyme using fluorescently labeled
998 lipids. *J. Bacteriol.* **192**, 5341-5349 (2010).
999 49. Lequette, Y., Lanfroy, E., Cogez, V., Bohin, J.P. & Lacroix, J.M. Biosynthesis of
1000 osmoregulated periplasmic glucans in *Escherichia coli*: the membrane-bound and the
1001 soluble periplasmic phosphoglycerol transferases are encoded by the same gene.
1002 *Microbiology* **154**, 476-483 (2008).
1003 50. Peschel, A. et al. Inactivation of the *dlt* operon in *Staphylococcus aureus* confers
1004 sensitivity to defensins, protegrins, and other antimicrobial peptides. *J. Biol. Chem.* **274**,
1005 8405-8410 (1999).
1006 51. Falagas, M.E., Rafailidis, P.I. & Matthaiou, D.K. Resistance to polymyxins: Mechanisms,
1007 frequency and treatment options. *Drug Resist. Updat.* **13**, 132-138 (2010).
1008 52. Djoko, K.Y., Ong, C.L., Walker, M.J. & McEwan, A.G. The role of copper and zinc
1009 toxicity in innate immune defense against bacterial pathogens. *J. Biol. Chem.* **290**,
1010 18954-18961 (2015).
1011 53. McDevitt, C.A. et al. A molecular mechanism for bacterial susceptibility to zinc. *PLoS*
1012 *Pathog.* **7**, e1002357 (2011).
1013 54. Buckland, A.G. & Wilton, D.C. Inhibition of secreted phospholipases A2 by annexin V.
1014 Competition for anionic phospholipid interfaces allows an assessment of the relative
1015 interfacial affinities of secreted phospholipases A2. *Biochim. Biophys. Acta* **1391**, 367-
1016 376 (1998).
1017 55. Hsu, Y.H., Dumlao, D.S., Cao, J. & Dennis, E.A. Assessing phospholipase A2 activity
1018 toward cardiolipin by mass spectrometry. *PLoS One* **8**, e59267 (2013).

1019 56. Koprivnjak, T., Peschel, A., Gelb, M.H., Liang, N.S. & Weiss, J.P. Role of charge
1020 properties of bacterial envelope in bactericidal action of human group IIA phospholipase
1021 A2 against *Staphylococcus aureus*. *J. Biol. Chem.* **277**, 47636-47644 (2002).
1022 57. Hunt, C.L., Nauseef, W.M. & Weiss, J.P. Effect of D-alanylation of (lipo)teichoic acids of
1023 *Staphylococcus aureus* on host secretory phospholipase A2 action before and after
1024 phagocytosis by human neutrophils. *J. Immunol.* **176**, 4987-4994 (2006).
1025 58. Carapetis, J.R., Steer, A.C., Mulholland, E.K. & Weber, M. The global burden of group A
1026 streptococcal diseases. *Lancet Infect. Dis.* **5**, 685-694 (2005).
1027 59. Goldstein, I., Rebeyrotte, P., Parlebas, J. & Halpern, B. Isolation from heart valves of
1028 glycopeptides which share immunological properties with *Streptococcus haemolyticus*
1029 group A polysaccharides. *Nature* **219**, 866-868 (1968).
1030 60. Ayoub, E.M. & Dudding, B.A. Streptococcal group A carbohydrate antibody in rheumatic
1031 and nonrheumatic bacterial endocarditis. *J. Lab. Clin. Med.* **76**, 322-332 (1970).
1032 61. Kirvan, C.A., Swedo, S.E., Heuser, J.S. & Cunningham, M.W. Mimicry and autoantibody-
1033 mediated neuronal cell signaling in Sydenham chorea. *Nat. Med.* **9**, 914-920 (2003).
1034 62. Shulman, S.T. et al. Group A streptococcal pharyngitis serotype surveillance in North
1035 America, 2000-2002. *Clin. Infect. Dis.* **39**, 325-332 (2004).
1036 63. Sumby, P. et al. Evolutionary origin and emergence of a highly successful clone of
1037 serotype M1 group a Streptococcus involved multiple horizontal gene transfer events. *J.*
1038 *Infect. Dis.* **192**, 771-782 (2005).
1039 64. Koga, T., Asakawa, H., Okahashi, N. & Takahashi, I. Effect of subculturing on
1040 expression of a cell-surface protein antigen by *Streptococcus mutans*. *J. Gen. Microbiol.*
1041 **135**, 3199-3207 (1989).
1042 65. Moore, G.E., Gerner, R.E. & Franklin, H.A. Culture of normal human leukocytes. *JAMA*
1043 **199**, 519-524 (1967).
1044 66. van de Rijn, I. & Kessler, R.E. Growth characteristics of group A streptococci in a new
1045 chemically defined medium. *Infect. Immun.* **27**, 444-448 (1980).
1046 67. Hoff, J.S., DeWald, M., Moseley, S.L., Collins, C.M. & Voyich, J.M. SpyA, a C3-like ADP-
1047 ribosyltransferase, contributes to virulence in a mouse subcutaneous model of
1048 *Streptococcus pyogenes* infection. *Infect. Immun.* **79**, 2404-2411 (2011).
1049 68. Caparon, M.G. & Scott, J.R. Genetic manipulation of pathogenic streptococci. *Methods*
1050 *Enzymol.* **204**, 556-586 (1991).
1051 69. Horton, R.M., Hunt, H.D., Ho, S.N., Pullen, J.K. & Pease, L.R. Engineering hybrid genes
1052 without the use of restriction enzymes: gene splicing by overlap extension. *Gene* **77**, 61-
1053 68 (1989).
1054 70. Trevino, J., Liu, Z., Cao, T.N., Ramirez-Pena, E. & Sumby, P. RivR is a negative
1055 regulator of virulence factor expression in group A Streptococcus. *Infect. Immun.* **81**,
1056 364-372 (2013).
1057 71. Kabsch, W. *Xds*. *Acta Crystallogr. D Biol. Crystallogr.* **66**, 125-132 (2010).
1058 72. Grosse-Kunstleve, R.W. & Adams, P.D. Substructure search procedures for
1059 macromolecular structures. *Acta Crystallogr. D Biol. Crystallogr.* **59**, 1966-1973 (2003).
1060 73. McCoy, A.J., Storoni, L.C. & Read, R.J. Simple algorithm for a maximum-likelihood SAD
1061 function. *Acta Crystallogr. D Biol. Crystallogr.* **60**, 1220-1228 (2004).
1062 74. Terwilliger, T.C. et al. Decision-making in structure solution using Bayesian estimates of
1063 map quality: the PHENIX AutoSol wizard. *Acta Crystallogr. D Biol. Crystallogr.* **65**, 582-
1064 601 (2009).
1065 75. Emsley, P., Lohkamp, B., Scott, W.G. & Cowtan, K. Features and development of *Coot*.
1066 *Acta Crystallogr. D Biol. Crystallogr.* **66**, 486-501 (2010).
1067 76. Afonine, P.V. et al. Towards automated crystallographic structure refinement with
1068 phenix.refine. *Acta Crystallogr. D Biol. Crystallogr.* **68**, 352-367 (2012).

1069 77. McCoy, A.J. et al. Phaser crystallographic software. *J. Appl. Crystallogr.* **40**, 658-674
1070 (2007).
1071 78. Adams, P.D. et al. *PHENIX*: a comprehensive Python-based system for macromolecular
1072 structure solution. *Acta Crystallogr. D Biol. Crystallogr.* **66**, 213-221 (2010).
1073 79. Chen, V.B. et al. *MolProbity*: all-atom structure validation for macromolecular
1074 crystallography. *Acta Crystallogr. D Biol. Crystallogr.* **66**, 12-21 (2010).
1075 80. Gore, S. et al. Validation of structures in the Protein Data Bank. *Structure* **25**, 1916-1927
1076 (2017).
1077 81. Schrodinger, LLC. The PyMOL Molecular Graphics System, Version 1.8.0.3. (2010).
1078 82. Bui, N.K. et al. Isolation and analysis of cell wall components from *Streptococcus*
1079 *pneumoniae*. *Anal. Biochem.* **421**, 657-666 (2012).
1080 83. Santander, J. et al. Mechanisms of intrinsic resistance to antimicrobial peptides of
1081 *Edwardsiella ictaluri* and its influence on fish gut inflammation and virulence.
1082 *Microbiology* **159**, 1471-1486 (2013).
1083 84. Ghomashchi, F. et al. Preparation of the full set of recombinant mouse- and human-
1084 secreted phospholipases A2. *Methods Enzymol.* **583**, 35-69 (2017).
1085 85. Le Breton, Y. & McIver, K.S. Genetic manipulation of *Streptococcus pyogenes* (the
1086 Group A Streptococcus, GAS). *Curr. Protoc. Microbiol.* **30**, Unit 9D 3 (2013).
1087 86. Le Breton, Y. et al. Genome-wide discovery of novel M1T1 group A streptococcal
1088 determinants important for fitness and virulence during soft-tissue infection. *PLoS*
1089 *Pathog.* **13**, e1006584 (2017).
1090 87. Anders, S. & Huber, W. Differential expression analysis for sequence count data.
1091 *Genome Biol.* **11**, R106 (2010).
1092 88. Robinson, M.D., McCarthy, D.J. & Smyth, G.K. edgeR: a Bioconductor package for
1093 differential expression analysis of digital gene expression data. *Bioinformatics* **26**, 139-
1094 140 (2010).
1095 89. Wagner, R. & Berger, S. Gradient-selected NOESY-A fourfold reduction of the
1096 measurement time for the NOESY Experiment. *J. Magn. Reson. A* **123**, 119-121 (1996).
1097 90. Willker, W., Leibfritz, D., Kerssebaum, R. & Bermel, W. Gradient selection in inverse
1098 heteronuclear correlation spectroscopy. *Magn. Reson. Chem.* **31**, 287-292 (1993).
1099 91. Kellogg, G.W. Proton-detected hetero-TOCSY experiments with application to nucleic
1100 acids. *J. Magn. Reson.* **98**, 176-182 (1992).
1101 92. Tsirigos, K.D., Peters, C., Shu, N., Kall, L. & Elofsson, A. The TOPCONS web server for
1102 consensus prediction of membrane protein topology and signal peptides. *Nucleic Acids*
1103 *Res.* **43**, W401-407 (2015).
1104 93. Soding, J., Biegert, A. & Lupas, A.N. The HHpred interactive server for protein homology
1105 detection and structure prediction. *Nucleic Acids Res.* **33**, W244-248 (2005).
1106 94. Edgar, R.C. MUSCLE: multiple sequence alignment with high accuracy and high
1107 throughput. *Nucleic Acids Res.* **32**, 1792-1797 (2004).
1108 95. Tamura, K., Stecher, G., Peterson, D., Filipski, A. & Kumar, S. MEGA6: Molecular
1109 Evolutionary Genetics Analysis version 6.0. *Mol. Biol. Evol.* **30**, 2725-2729 (2013).

1110